Nonlinear targeted energy transfer of two coupled cantilever beams coupled to a bistable light attachment

P.-O Mattei, R Ponçot, M Pachebat, Renaud Côte

Nonlinear Targeted Energy Transfer of Two Coupled Cantilever Beams Coupled to a Bistable light Attachment.

P.-O. Mattei[a,*], R. Ponçot[b], M. Pachebat[a], R. Côte[a]

[a]*LMA, CNRS, UPR 7051, Aix-Marseille Univ, Centrale Marseille, 4 impasse Nikola TESLA, CS 40006,13453 Marseille Cedex 13, France*

[b]*Parrot SA, 174 quai de Jemmapes, 75010 Paris, France*

Abstract

In order to control the sound radiation by a structure, one aims to control vibration of radiating modes of vibration using "Energy Pumping" also named "Targeted Energy Transfer". This principle is here applied to a simplified model of a double leaf panel. This model is made of two beams coupled by a spring. One of the beams is connected to a nonlinear absorber. This nonlinear absorber is made of a 3D-printed support on which is clamped a buckled thin small beam with a small mass fixed at its center having two equilibrium positions. The experiments showed that, once attached onto a vibrating system to be controlled, under forced excitation of the primary system, the light bistable oscillator allows a reduction of structural vibration up to 10 dB for significant amplitude and frequency range around the first two vibration modes of the system.

Keywords: Noise Reduction, Energy Pumping, Nonlinear Absorber, Bi-stable Attachment, Buckled Beam.

1. Introduction

Despite active work along the years, reducing noise is an attractive topic because it allows, for example, improved fatigue resistance with a consequent reduction in maintenance costs and noise reduction resulting in increased comfort. Many active and passive devices have been developed to improve the vibroacoustic behaviour of mechanical assemblies such as double-leaf walls.

In the passive domain, for example, the absorption of acoustic waves is typically accomplished through the absorbent material placed on the domain walls. The effectiveness of the device depends strongly on the frequency of the waves to be absorbed. To mitigate structural vibration, the Frahm absorber [1], consisting of a mass-spring-damper system, tuned to the frequency of vibration to eliminate is very efficient but has a limited frequency range of effectiveness [2]. Passive nonlinear Energy Pumping is a way to overcome such a limitation. Since the seminal work by Gendelman *et al.* [3, 4], because of its various and numerous applications, the problem of passive nonlinear energy pumping has become a subject of growing interest [5]. The simplest case requires consideration of a linear mechanical or acoustical system connected to a secondary oscillator having a strongly non linear stiffness (typically a cubic one). This attachment is usually termed as nonlinear Energy Sink (NES). This kind of non linearity corresponds to a resonance of the NES that varies with the amplitude of excitation. This enables a passive non linear energy transfer that is realized through resonance capture at high energy value [4]. Passive non linear energy transfer from the primary system to the NES occurs under resonance condition once the NES amplitude rises above a certain

*Corresponding author

Email addresses: mattei@lma.cnrs-mrs.fr (P.-O. Mattei), remi.poncot@parrot.com (R. Ponçot), pachebat@lma.cnrs-mrs.fr (M. Pachebat), cote@lma.cnrs-mrs.fr (R. Côte)

threshold; reverse energy flow from the NES to the primary system is prevented because of resonance escape due to the energy decrease induced by dissipation. The existence of such threshold in purely cubic or quintic NES can be viewed either as advantage either as disadvantage depending upon application. But the main feature of energy pumping lies in the fact that the higher the frequency of the primary linear system to control, the higher the amplitude for efficient non linear passive dissipation.

To date a wide variety of NESs have been proposed and tested: pure cubic spring in mechanical systems [5], membrane acting as cubic or quintic spring in acoustical systems [6], loudspeaker used as a suspended piston acting as an essentially nonlinear oscillator [7]. A numerical work by Gourdon and Lamarque [8] suggest that a NES described by a nonlinear Duffing equation with negative stiffness, acting as a chaotic system, is able to achieve energy pumping for low energy level. The recent theoretical and numerical work by Savadkoohi *et al* [9] and Manevitch *et al* [10, 11] showed that a bi-stable nonlinear oscillator manifests significant advantages with respect to energy pumping efficiency. We have developed an experimental nonlinear bi-stable absorber made of a small mass fixed at the midspan of a buckled beam, similar to that proposed in [11], that provides improved efficiency in frequency and excitation range over existing passive devices.

In order to control the sound radiation by a panel, one aims to control vibration of radiating modes of vibration using energy pumping. This principle is here applied to a simplified model of a double leaf panel. This model is made of two beams coupled by a spring. One of the beams is connected to the nonlinear resonator. This nonlinear resonator is made of a 3D-printing support on which is clamped a buckled thin beam with a mass fixed at its middle. The main feature of this nonlinear resonator lies in the buckling that allows a bi-stable comportment easy to control, in the following it is denoted by bi-stable attachment (BSA) . Our experimentations show that this simple device leads up to more than 10 dB attenuation for the first two vibration modes of the system.

An optimization made on a simplified model of the device by a parametric study of the influence of dissipation is conducted. We show that for a wide range of configurations with one nonlinear dynamic absorbers, a reduction up to more than 10 dB of the vibration of the primary system around its first two resonances is obtained.

Sec. 2 is devoted to the description of the experiment. In Sec. 3 a simplified model is established. In Sec. 4 experimental and numerical results show the efficiency of the nonlinear absorber to attenuate the vibration of the primary linear system. The conclusions are given in Sec. 5.

2. Experimental Fixture

Since our aim was to describe the main feature of a double leaf wall close to its mass-air-mass resonance, we have chosen to make a simplified but representative experiment. A photograph of the fixture is given in Fig. 1 and a sketch of it is given in Fig. 2. Each panel is replaced by a cantilever viscously damped beam whose dimension had been chosen to recover the feature of the panel. Each beam is made of steel with Young modulus $E_b = 185$ GPa, volume mass density $\rho_b = 7621$ kg/m^3 and viscous damping $\mu_b = 0.1$ kg/s. Its dimensions are given by its thickness that is $h_b = 4.2$ mm and its height that is $e_b = 2.52$ cm ; its length $L = 35$ cm is comparable to the half size of a double leaf panel made with BA13 plaster plates fixed on vertical studs whose spacing is generally recommended to be close to 60 cm. The two beams are connected by a coupling spring with mass $m_c = 6$ g and stiffness $r_c = 2200$ kg.s^{-2} corresponding to the stiffness of the air gap separating two panels in usual conditions. This spring is located close to the free end of the beams at $x_N = 34.5$ cm. The excitation is made by a non-contact driver located at $x_0 = 3.5$ cm

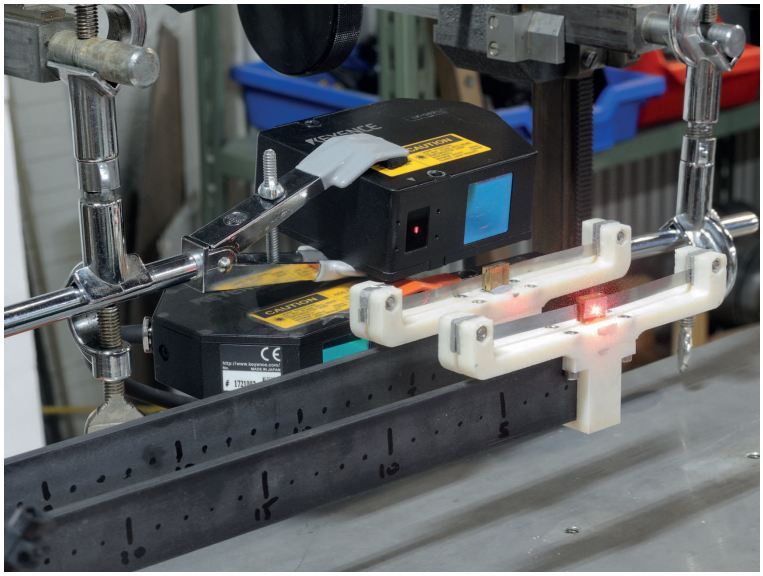

Figure 1: Photograph of the experiment. In that experiment, only one BSA is active. The second remains fixed.

of the clamped end of a beam. The BSA consists in a small mass (here a mass $m_0 = 2.6$ g had been chosen) fixed at the middle of very thin buckled viscously damped steel beam with Young modulus $E = 200$ GPa and volume mass density $\rho = 7800$ kg/m^3 ; its length is $\ell = 10$ cm, its thickness is $h = 0.1$ mm and its height is $e = 5$ mm. The buckled beam is rigidly fixed at its ends to an ABS (Acrylonitrile Butadiene Styrene) support made by a 3D-printer. The support is fixed close to the end the cantilever beam at $x_N = 34.5$ cm. The total weight of the each BSA is $M_N = 32$ g. It is worth noting that the viscosity of BSA buckled beam can be defined in line with that of the primary one as $\mu = 0.1$ kg/s, but as shown later on, most of the damping of the BSA is induced by its support and the actual value of the BSA damping will be deduced from experimental measurement. To ensure a symmetry in the system a support is fixed at the end of each of the cantilever beam, but only one supports an active BSA, the other remains blocked all along the experiment.

The first two modes of this system are obtained for the in-phase (close to 22 Hz) and the out-of-phase (close to 39 Hz) movement of the first mode of each cantilever beam. The displacement of the cantilever beam is measured by a Keyence CCD Laser Displacement Sensor LK-G 32. The displacement of the BSA is measured by a a Keyence CCD Laser Displacement Sensor LK-G 82 and its velocity by Polytech Laser Doppler Vibrometer OVF-303.

3. Simplified Model of the Fixture

Since our aim is to study the nonlinear dynamics of the system around its two first modes, we have chosen to approximate the continuous model by a simplified three or four degrees of freedom (dof) that capture the main features of the physical device. As can be seen below, despite the strong approximations, this simplified model is able to recover the whole dynamics of the experimental fixture. This allows to make a simplified parametric study able to put in light the

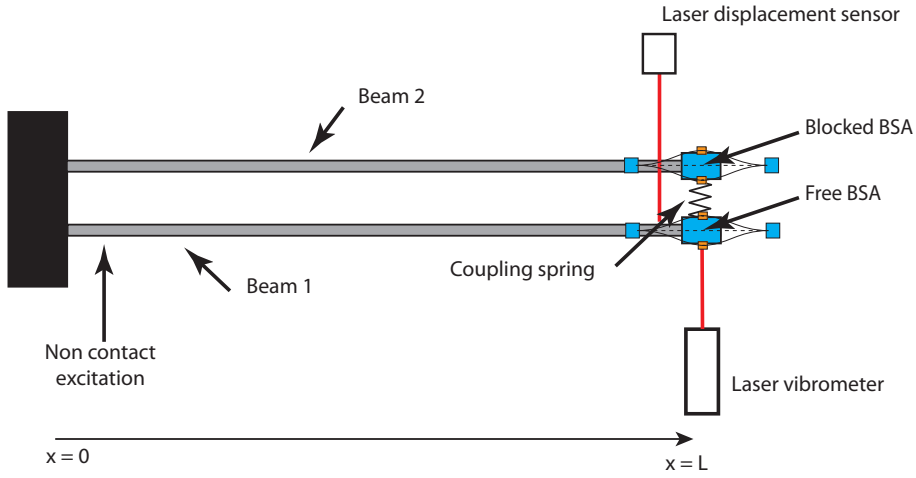

Figure 2: Sketch of the experiment.

principal parameters acting on the system. We start by presenting the model of the two coupled cantilever beams with a BSA attached close to their free ends. The second part is devoted to the damped buckled beam approximation for the BSA, its limits and the way to overcome them.

3.1. Approximation of the coupled beams displacement

Let us consider two identical cantilever beams (denoted hereafter by beam 1 and beam 2) coupled by a spring close to their free ends at $x = x_N$. This spring has a stiffness r_c and a mass m_c. To simplify, one can consider that half of the spring mass is attached to each beam. Also, a point mass M_N is fixed at $x = x_N$. Under the classical Euler-Bernoulli hypothesis, if only the first beam if excited by an external force, the displacement of the beams $w_1(x,t)$ and $w_2(x,t)$ are the solutions of

$$\begin{aligned} E_b I_b \frac{\partial^4 w_1(x,t)}{\partial x^4} + \mu_b \frac{\partial w_1(x,t)}{\partial t} + \left(\rho_b S_b + \left(M_N + \frac{m_c}{2}\right)\delta_{x_N}(x)\right)\frac{\partial^2 w_1(x,t)}{\partial t^2} & \\ + r_c \delta_{x_N}(x)\left(w_1(x,t) - w_2(x,t)\right) &= F(t)\delta_{x_0}(x), \end{aligned} \tag{1}$$

$$\begin{aligned} E_b I_b \frac{\partial^4 w_2(x,t)}{\partial x^4} + \mu_b \frac{\partial w_2(x,t)}{\partial t} + \left(\rho_b S_b + \left(M_N + \frac{m_c}{2}\right)\delta_{x_N}(x)\right)\frac{\partial^2 w_2(x,t)}{\partial t^2} & \\ - r_c \delta_{x_N}(x)\left(w_1(x,t) - w_2(x,t)\right) &= 0, \end{aligned} \tag{2}$$

with $I_b = e_b h_b^3/12$ and $S_b = e_b h_b$. $\delta_{x_N}(x)$ is the Dirac delta distribution located at $x = x_N$. If $H_t(t)$ is the Heaviside unit step function, then one defines $F(t) = AH_t(t)\cos(\omega t)$ as the sinusoidal forcing at a frequency f starting at $t = 0$. $\omega = 2\pi f$ is the angular frequency. To these equations, one adds initial conditions $w_{1,2}(x, t = 0) = 0$ and $\partial w_{1,2}(x, t = 0)/\partial t = 0, \forall x \in [0, L]$ and boundary conditions for the displacement $w_{1,2}(x = 0, t) = 0$, $\partial w_{1,2}(x = 0, t)/\partial x = 0$, $\partial^2 w_{1,2}(x = L, t)/\partial x^2 = 0$, $\partial^3 w_{1,2}(x = L, t)/\partial x 3 = 0, \forall t \geq 0$.

Since only low frequency movement is considered, the two coupled beams dynamics is described by a simplified system with two degrees of freedom. At low frequency, each displacement $w_{1,2}(x,t)$

is expanded as $w_{1,2}(x,t) = \phi_1(x)u_{1,2}(t)$, where $\phi_1(x)$ is the first mode of the cantilever beam. Introducing these expansions in the two coupled equation 1 and 2 together with a Ritz reduction leads to a system of two coupled differential equations:

$$\begin{aligned} m_1\ddot{u}_1(t) + \mu_b\dot{u}_1(t) + k_1u_1(t) + k_c(u_1(t) - u_2(t)) &= \phi_1(x_0)F(t) \quad (3)\\ m_1\ddot{u}_2(t) + \mu_b\dot{u}_2(t) + k_1u_2(t) - k_c(u_1(t) - u_2(t)) &= 0, \quad (4)\end{aligned}$$

$\dot{u}_i(t)$ is the time derivative of each component $u_i(t)$. In these equations $m_1 = \rho_b S_b + \left(M_N + \frac{m_c}{2}\right)\phi_1^2(x_N)$ represents the total dynamic mass and $k_c = r_c\phi_1^2(x_N)$ the dynamic coupling stiffness.

3.2. Approximation of the BSA displacement

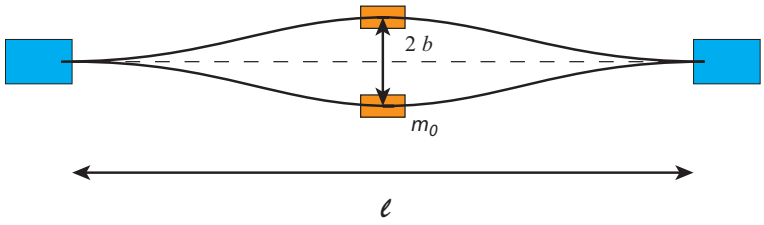

Figure 3: Sketch of the BSA geometry.

A thin viscously damped fixed-fixed beam with a small mass m_0 fixed at its center when buckled under axial constraint N has a geometric nonlinearity. Thereafter, one considers that, in our case, the axial load is in-between the first two critical loads, allowing only the first stable buckled mode to exist. Then the beam has a static buckled configuration with two symmetrical equilibrium positions as presented in Fig. 3. b is the rise at the midspan of the beam that depends on the constraint N. Accounting for thin structure large displacement is classically made by using the Von Kármán's nonlinear plate theory [12, 13, 14]. As shown in the Appendix A, a simple change of variable together with a Ritz reduction transforms the nonlinear partial differential equation governing the beam displacement dynamics of the BSA into a one dof Helmholtz-Duffing nonlinear equation for the non-dimensional BSA displacement $\tilde{q}(\tilde{t})$:

$$(3/8+\beta)\ddot{\tilde{q}}(\tilde{t}) + \frac{3}{8}\tilde{\mu}\dot{\tilde{q}}(\tilde{t}) + \frac{\tilde{b}^2\pi^4}{4}\left(\tilde{q}(\tilde{t}) + \frac{3}{2}\tilde{q}(\tilde{t})^2 + \frac{1}{2}\tilde{q}(\tilde{t})^3\right) = \frac{1}{\tilde{b}^2}H_{\tilde{t}}(\tilde{t})\cos(\tilde{\omega}\tilde{t})\int_0^1 \tilde{F}(\tilde{x})\tilde{w}_0(\tilde{x})\mathrm{d}\tilde{x} \quad (5)$$

It is easy to show that this equation has three equilibrium points. Two are stable (0 and -2) corresponding to each buckled position. One is unstable (-1).

The obvious counterpart of the simplified description of the buckled beam dynamics is that this single mode approximation does not allow to describe the whole dynamics of the BSA. A simple linear analysis of the buckled beam, obtained by dropping the quadratic and cubic terms in Eq. (5), leads to a linear resonance frequency of $\tilde{b}\frac{\pi^2}{2}/\sqrt{\frac{3}{8}+\beta}$ that shows a linear dependence in $\tilde{b}$. Since in our case, $\tilde{b} \approx 81$, we obtain a physical value of $\check{f}_{Nl}^{th} \approx 352$ Hz. The measurement of the first natural linear resonance of the BSA gives $\check{f}_{N1}^{e} \approx 36$ Hz. This shows an obvious strong deviation of the theoretical model from the experimental one. As observed by Kreider and Nayfeh [13], the single mode approximation is valid only for very low values of $\tilde{b} < 2$. If one computes the exact

linear undamped natural frequencies for a buckled beam [13], one obtains for $\tilde{b} \approx 81$ an exact value of about $\check{f}_{Nl}^{th} \approx 39.7$ Hz, closer to the measured one. It is worth noting that the point mass at the beam centre lowers the natural frequencies of the symmetric buckling modes. Since our aim is to keep the model as simple as possible, we have decided to retain Eq. (5) but with its physical parameter (stiffness and damping) estimated from a measure of the first linear resonance of the BSA. As presented in the next paragraph for the linear coupled beams, one obtains the experimental linear resonance by identification of the linear response of the BSA around its first resonance to a Lorentzian singly peaked function. One obtains $f_{N1} = \check{f}_{N1} - \imath\hat{f}_{N1} \approx 35.7 - \imath 0.3$ Hz. The value of the damping ratio $\zeta = \hat{f}_{N1}/\check{f}_{N1} \approx 0.8\%$ is about 20 times greater than steel's natural damping, since it is of the same order as that of the BSA support damping which is made of ABS and which has been measured close to 1.5%, most of the BSA's damping is given by its support.

Then returning to the physical parameter, one obtains the following nonlinear differential equation for the BSA movement $q(t)$

$$m_N \ddot{q}(t) + \mu_N \dot{q}(t) + k_N \mathcal{F}\left(q(t)\right) = \mathcal{A} H_{\tilde{t}}(\tilde{t}) \cos(\tilde{\omega}\tilde{t}), \tag{6}$$

where $m_N = (3/8\rho A\ell + m_0)$ is the dynamic mass, $\mu_N = 4\pi m_N \hat{f}_{N1}$ is the identified dynamic damping and $k_N = (2\pi \check{f}_{N1})^2 m_N$ is the identified dynamic stiffness. In this equation, the non linear stiffness is given by $\mathcal{F}\left(q(t)\right) = (q(t) - b) + 3/(2b)\left(q(t) - b\right)^2 + 1/(2b^2)\left(q(t) - b\right)^3$. The solution of this equation was calculated without any particular difficulty under the Mathematica [15] software by using the built-in numerical differential equation solving function "NDSolve".

This BSA was fixed to a measurement shaker. In order to measure its velocity nonlinear frequency response function, the following experimental procedure had been set on: the excitation frequency varies from 13 Hz to 40 Hz using 101 frequency steps while the amplitude varies from 0.1 V to 1.25 V using 24 voltage steps. For each pair frequency/amplitude the signal is set on, 10 s after the beginning of the signal, the time record starts at a sampling rate of 4096 Hz for a duration of 10 s. 7 s after the beginning of the recording, the excitation is stopped. This procedure allows recording 7 s of stabilized signal and 3 s of transient state. After the end of the recordings, the BSA returns to one of its equilibrium position. Then one waits 10 s more to keep the system calm. Each measurement takes 30 s, allowing an experimental set to be completed by 12 hours. The velocity of the moving mass located at the middle of the BSA was measured using a non contact laser vibrometer (Polytech OVF-303). When necessary, the velocity data was converted to displacement using numeric integration using the cumulative trapezoidal numerical integration function in Matlab.

One presents below three-dimensional plots of the measured (see Fig. 4 (a)) and computed (see Fig. 4 (b)) frequency response for the displacement of the mass at the middle of the BSA. In both cases the frequency response was computed using a root mean square value (RMS) of the displacement over the RMS amplitude excitation. These RMS values were calculated by taking the last three seconds of the 7 s long stabilized signal. For the two figures, the frequency ranges from 13 Hz to 40 Hz using 101 frequency steps while, since there is no clear correspondence between the excitation amplitude for the model and the experimental one, the amplitude range of the model was adjusted to fit with that of the experiment, here 24 amplitude steps were used for the model to be in line with the experimental set up.

This result shows that on the whole, the simplified 1 d-o-f model is able to recover the main features of the BSA: softening a low amplitude, resonance at 1/2 the natural frequency induced by the quadratic non linear term, strong displacement values for a large amplitude-frequency domain, chaotic movement over a large amplitude-frequency range. Obviously some features are not captured

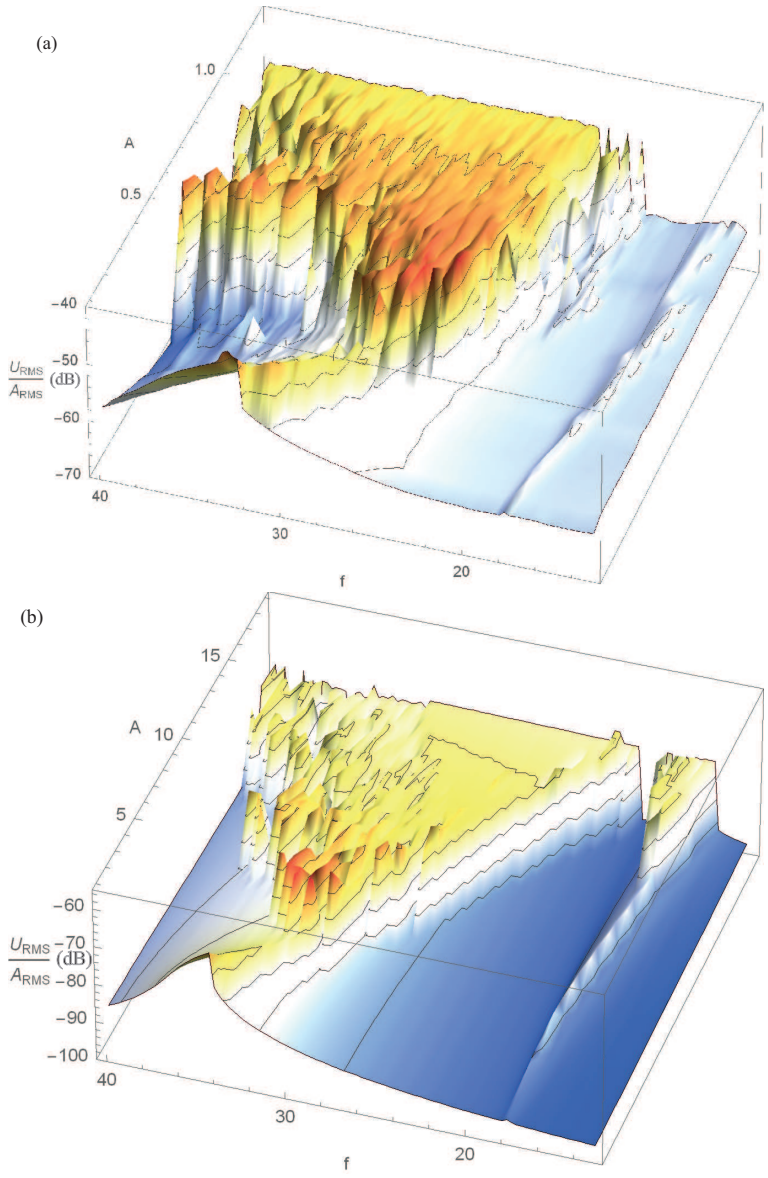

Figure 4: Frequency response of the RMS value for the measured (a) and computed (b) BSA displacement $20\log(\tilde{q}_{RMS}/A_{RMS})$ vs frequency and amplitude. On both curves, the thin black curves are separated by 5 dB.

by this simplified model: the strong displacement values computed do not fit well with the measured ones at the highest frequencies, also the damping model is not satisfactory since while the value for the BSA damping, which was estimated from the linear resonance, gives satisfactory results at low amplitude, it should have been increased to keep $\tilde{q}_{RMS}/A_{RMS}$ in line with the highest amplitude of the experimental data, but in that case the damping model could not have been described by

the viscous linear model used here. To see in more details the measured and computed behaviour, we present in the Appendix B results for some chosen experimental amplitude-frequency pairs and their corresponding computed pairs.

3.3. The full system

The complete system corresponding to the two coupled primary beams (with displacement $u_1(t)$ and $u_2(t)$) solution of equations 3 and 4) with two BSAs fixed at each primary beam end (with displacement $\tilde{q}_1(t)$ and $\tilde{q}_2(t)$, solution of Eq. (6)) is given by

$$\begin{aligned}
m_1\ddot{u}_1(t) + \mu_1\dot{u}_1(t) + k_1u_1(t) + k_c(u_1(t) - u_2(t)) & & \\
-\mu_N\left(\dot{q}_1(t) - \phi_1(x_N)\dot{u}_1(t)\right) - k_{1N}\mathcal{F}\left(q_1(t) - \phi_1(x_N)u_1(t)\right) &= A\phi_1^2(x_0)F(t) & (7)\\
m_1\ddot{u}_2(t) + \mu_1\dot{u}_2(t) + k_1u_2(t) - k_c(u_1(t) - u_2(t)) & & \\
-\mu_N\left(\dot{q}_2(t) - \phi_1(x_N)\dot{u}_2(t)\right) - k_{2N}\mathcal{F}\left(q_2(t) - \phi_1(x_N)u_2(t)\right) &= 0 & (8)\\
m_N\ddot{q}_1(t) + \mu_N\left(\dot{q}_1(t) - \phi_1(x_N)\dot{u}_1(t)\right) + k_{1N}\mathcal{F}\left(q_1(t) - \phi_1(x_N)u_1(t)\right) &= 0 & (9)\\
m_N\ddot{q}_2(t) + \mu_N\left(\dot{q}_2(t) - \phi_1(x_N)\dot{u}_2(t)\right) + k_{2N}\mathcal{F}\left(q_2(t) - \phi_1(x_N)u_2(t)\right) &= 0 & (10)
\end{aligned}$$

with $F(t) = AH_t(t)\sin(\omega t)$, where A is the given excitation amplitude. When a BSA is not active as in the experimental results presented below, only the BSA fixed on the excited beam is active while the other remains blocked, then the system of four coupled nonlinear differential equations given by Eq. (7), (8), (9) and (10) is simply reduced to a three-equations system given by Eq. (7), (9) and (8) in which not only the non linear term $k_{2N}\mathcal{F}\left(q_2(t) - \phi_1(x_N)u_2(t)\right)$ but also the viscous term $\mu_N\dot{u}_2(t)$ had been deleted.

The solutions $u_1(t)$, $u_2(t)$ and $q_1(t)$ of the system given by Eq. (7), (8) and (9) were also calculated without any particular difficulty under the Mathematica[15] software by using the built-in numerical differential equation solving function "NDSolve". It is worth noting that all the mechanical parameters for both beams and BSA given in the previous section are the same except the linear resonance of the BSA that has slightly changed during the installation of the BSA on the beam. Its real part was measured as $\check{f}_N \approx 29$ Hz and its imaginary part was estimated from the previous measurement as $\hat{f}_N \approx 0.26$ Hz.

To validate all these approximations, we have done a comparison of the first two measured and computed resonance frequencies of the system when excited at very low amplitude to ensure a linear comportment.

To do so, around each resonance, we have estimated each of the two complex resonances as a complex value $f_i = \check{f}_i - \imath\hat{f}_i$, $i = 1, 2$. This approximation is valid in the present case since, for sufficiently separated modes, a linear vibrating system can be approximated by a one dof damped oscillator $m\ddot{u}(t) + c\dot{u}(t) + ku(t) = 0$, of mass m, viscous damping c and stiffness k. It is obvious that such an oscillator has a complex resonance $2\pi f = \omega$ that is given by $\omega = \pm\sqrt{k/m + c^2/(4m^2)} - \imath c/(2m) = \pm\check{\omega} - \imath\hat{\omega}$. It is worth noting that for such an oscillator with small damping, the damping ratio $\zeta = 1/2c/\sqrt{mk} \approx \hat{\omega}/\check{\omega}$. Then, it is sufficient to measure or compute the normalized frequency response function (FRF) of the system around each resonance and to estimate $f_i = \check{f}_i - \imath\hat{f}_i$, $i = 1, 2$ by fitting the FRF by a Lorentzian singly peaked function $A_i/\left|f^2 - f_i^2\right|$, $i = 1, 2$. In the present case, the displacement amplitude normalised by the excitation amplitude of the beam 2 had been measured and computed at a given very low excitation amplitude when varying the excitation frequency. The fitting had been made using Mathematica [15] software by using the

built-in standard fitting procedure without any difficulty. An example of measured FRF around the first mode and the identified Lorentzian is given in Fig. 5.

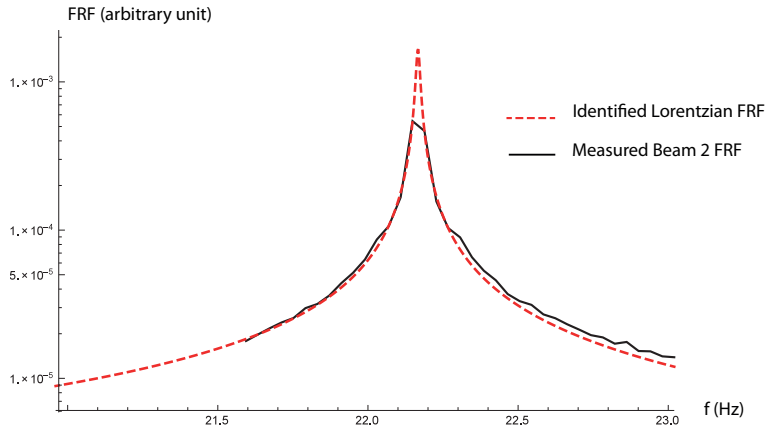

Figure 5: Example of linear modal identification. The black continuous curve represents experimental FRF of beam 2. The red discontinuous curve represents the identified Lorentzian with frequency $f_1^e = 22.2 - \imath 0.006$ Hz

One obtains for the experimental resonances $f_1^e = 22.2 - \imath 0.006$ Hz and $f_2^e = 39.3 - \imath 0.023$ Hz. At very low amplitude, to ensure a linear movement for the BSA, one obtains for the system given by equations 7, 8 and 9 the computed resonances $f_1^c = 22 - \imath 0.015$ Hz and $f_2^c = 39 - \imath 0.031$ Hz. The very good agreement indicates that not only the mechanical and geometrical characteristics are well identified but that the simplified 3 dof is able to recover the fine details of low frequency dynamics of the two coupled beams. It is worth noting that the damping ratio of the system, close to 0.05 %, is very small and mainly induced by the damping in the two coupled linear beams. For such an underdamped system, the oscillations take a rather significant time, ie several seconds, to vanish. In the present configuration, the BSA has little effect on the system, it only slightly shift the two linear resonances of the primary system ; obviously if its resonance is chosen close to one of the linear system, a shift of it is observed and the BSA acts as a Frahm absorber [1, 2].

4. Results

4.1. Attenuation of the FRF around the first two modes

As already said, in the experiments reported here, only the BSA fixed on beam 1 was active. Around each mode of the primary system (that is 22.2 Hz and 39.3 Hz), a set of beam 1 displacement frequency response (FR) had been measured with a stepped sine source at constant amplitude. The sinusoidal forcing signal had a duration of 30 s, enough to reach stable movement for the primary system at a given amplitude and frequency. Only the last three seconds of the forced movement were used to compute the RMS value of the displacement of the beam. After that, the source was switched off and it has been waiting for 20 s, enough for the vibration of both beams to vanish, before beginning a new measure. The lowest excitation amplitude had been fixed in order to ensure a linear comportment of the whole system (coupled beams and BSA). The highest excitation amplitude chosen ensures a linear comportment of the coupled beams (in that case, the maximum amplitude at their free ends remained much smaller than their thickness). The experimental and

numerical ranges were fixed to the following: around the first mode the frequency ranges from 21 Hz to 23 Hz with 53 steps while the experimental amplitude varies from 0.05 V to 2 V using 30 voltage steps and the numeric amplitude A was fixed to vary from 0.01 to 2 using 30 steps ; around the second mode the frequency ranges from 38 Hz to 40 Hz with 53 steps while the experimental amplitude varies from 0.1 V to 2.5 V using 25 voltage steps and the numeric amplitude A varies from 0.1 to 3.5 using 25 steps. It is worth noting that around each mode, the numeric amplitude range was fitted to give the best correspondence with experimental results. Obviously, in the results presented in Fig. 6 for the first mode around 22 Hz and in Fig. 7 for the second mode around 39 Hz, the results were obtained for a BSA that remains unchanged.

In these figures the difference between two successive thin horizontal black lines corresponds to a change in level by 5 dB. Each point of the surface corresponds to a given amplitude/frequency pair, the quantity plotted is the ratio of the RMS value calculated on the last 3 seconds of the signal of the displacement and of the excitation, that is $20 \log U_{RMS}/A$, where $U_{RMS} = \sqrt{1/3 \int_{t_1-3}^{t_1} u_1^2(t)\mathrm{d}t}$ is the measured beam 1 displacement and $A = \sqrt{1/3 \int_{t_1-3}^{t_1} A^2(t)\mathrm{d}t}$ is the measured excitation amplitude, the time t_1 correspond to the time just before the source switch off. These results show that when the BSA is activated, the energy pumping lowers the response of the primary system up to 10 dB.

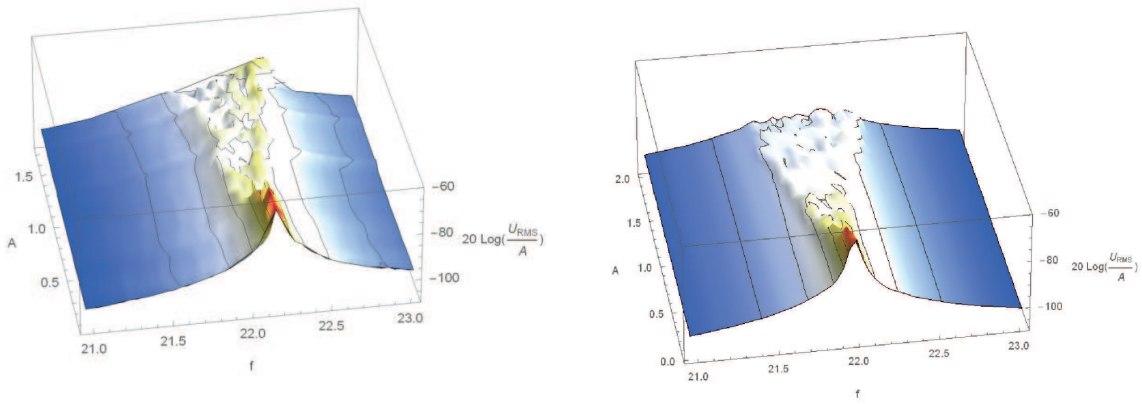

Figure 6: Surface plot of beam 1 displacement frequency response around the first mode. Left: measurement, right: model

It is worth noting that, in the results presented here, the higher the excitation amplitude the lower the relative response of the primary system. These results show that, not only a light BSA (the weight of the moving part of the BSA is 3 g and its supports is about 35 g) is able to significantly reduce the vibratory amplitude of a quite heavy system (it weighs about 0.6 kg), but also that despite all hypothesis, the simplified model is able to recover most of the features of the system : a small shift of the frequency of the firsts two modes of the primary system, spreading and lowering of the FR up to 10 dB.

To see it more clearly, one presents in Fig. 8 for the first mode around 22 Hz and in Fig. 9 for the second mode around 39 Hz the ridge curves for these results. The ridge curve is defined as the curve connecting the maxima of each frequency response, each point showing the maximal

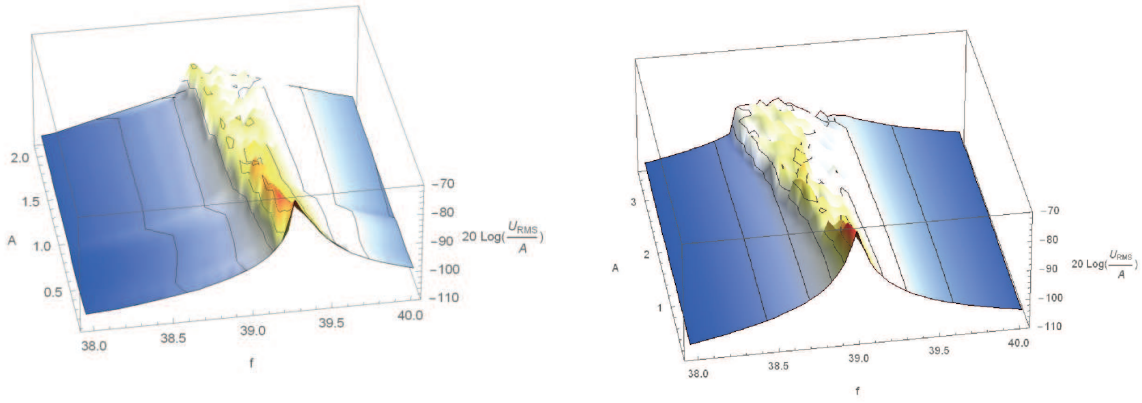

Figure 7: Surface plot of beam 1 displacement frequency response around the second mode. Left: measurement, right: model

frequency response amplitude of beam 1 displacement observed for a given excitation amplitude. In these figures, the red line corresponds to the ridge curve of the associated linear system which is a straight line. The experimental linear ridge curve is estimated by drawing a straight horizontal line from the maximum FR obtained from the lowest amplitude. The numerical one is obtained in a similar way ; the linear FR is obtained by cancelling the nonlinearity in the BSA equation. While details are not perfectly recovered, in particular the first mode attenuation is a bit overestimated, on the whole most of the features of energy pumping are obtained. It is worth noting that one of the difficulty of such an experiment is ensuring its long term stability since each experiment lasts about 20 hours; the fixture is very robust since all along these experiments, without any particular action undertaken to ensure stability of the system parameters (mainly the buckling of the thin beam), the system has shown a very good repeatability.

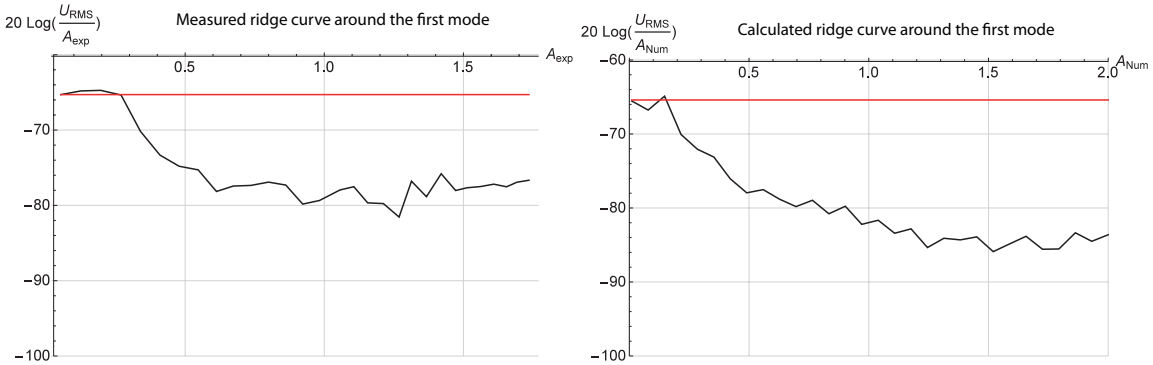

Figure 8: Ridge curve of beam 1 displacement frequency response around the first mode. Left: measurement, right: model. The straight line corresponds to the ridge curve for the linear BSA.

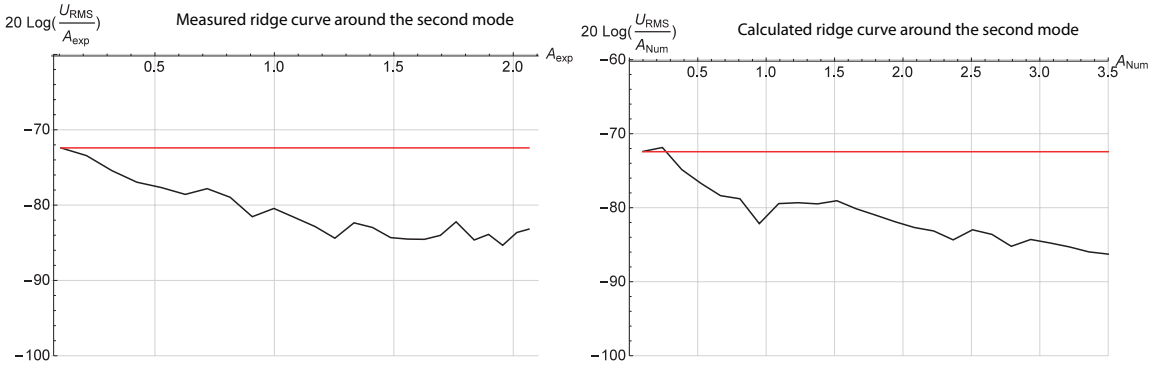

Figure 9: Ridge curve of beam 1 displacement frequency response around the second mode. Left: measurement, right: model. The straight line corresponds to the ridge curve for the linear BSA.

We present in Fig. 10 to 15 results for some characteristic experimental beam and BSA response for fixed amplitude-frequency pairs around the two modes of linear system. Each of these plots is composed of four sub-plots: the (a) plot shows the location of the point of interest in the density plot (corresponding to an upside view of the two experimental frequency response around the first mode given in Fig. 6 and second mode in Fig. 7) as a black oval, the (b) plot shows a phase plot (displacement/velocity) for the BSA in which the equilibrium points had been represented as black circles, the (c) curve shows the spectrum of the normalised BSA displacement and the (d) curve shows the spectrum of the normalised beam 1 response signal.

The first set of typical results around the first mode for the linear system is given in Fig. 10 and 12. The results presented in Fig. 10 correspond to the linear response of the system; in that case, the BSA was not active, while showing a very small nonlinear response. The results presented in Fig. 11 correspond to the activation of the BSA (allowing an overall attenuation of the frequency response of the linear system of about 6 dB), it has a quasi periodic response; the response of the linear system was no longer perfectly periodic as the BSA response has spread the energy over the whole spectrum; in that case, the second mode of the linear system has a amplitude 20 dB below that of the first mode.The results presented in Fig. 12 shows that the BSA was activated (allowing an overall attenuation of the frequency response of the linear system of more than 10 dB) with a chaotic motion around its two equilibrium positions in line with that predicted by Romeo et al. [11] for transient dynamics. This spreading of the energy over the whole spectrum, not so obvious to observe on these results because the displacement laser sensors are limited to the low frequency domain (more or less below 300 Hz), has excited the high frequency modes of the linear system. It is worth noting that, in the present case, the peak level of the second mode of the linear system remained at least 10 to 15 dB below that of the main peak.

The second set of typical results is obtained around the second mode for the linear system and it is given in Fig. 13, 14 and 15. On the whole, the interpretation of these results is similar to that done for the first mode. The results presented in Fig. 13 correspond to the linear response of the system; in that case, the BSA is not active, while showing a small nonlinear response. The results presented in Fig. 14 correspond to the activation of the BSA (allowing an overall attenuation of the frequency response of the linear system of about 6 dB), it has a quasi periodic response and again, the response of the linear system is not perfectly periodic since the BSA response has spread the energy over the whole spectrum, in that case, the fist mode of the linear system has a amplitude 30

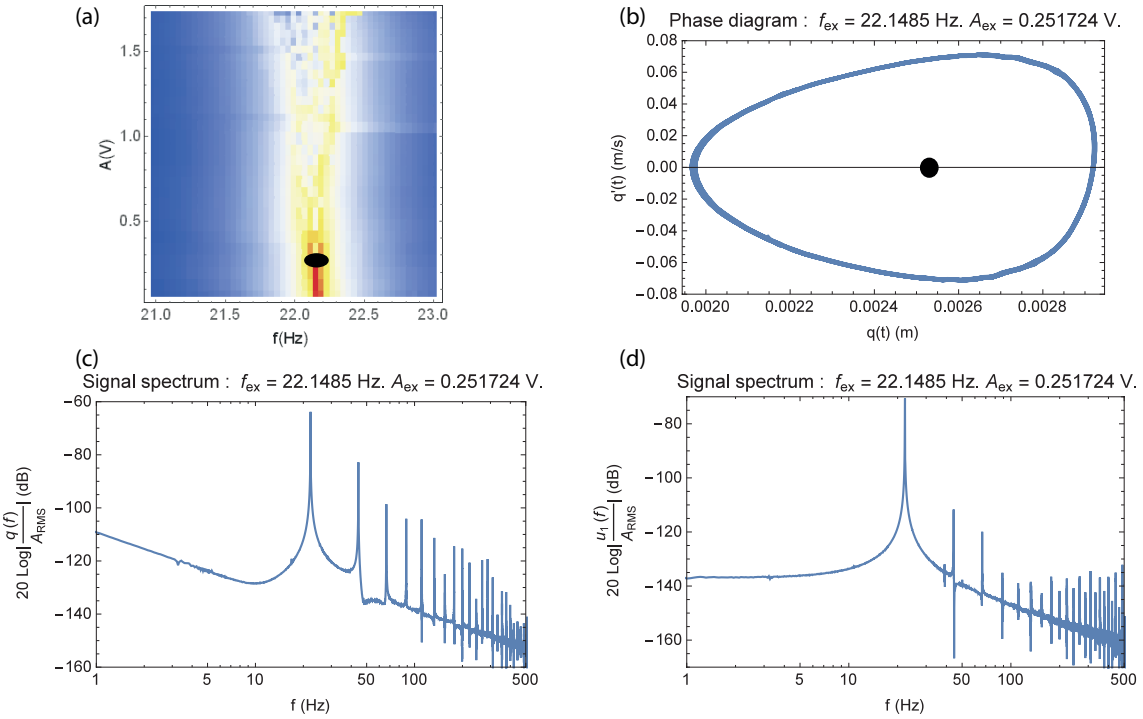

Figure 10: Typical measured system response around the linear system first mode at an excitation frequency $f_{ex} \approx$ 22.15 Hz and amplitude $A_{ex} \approx 0.3925$ V. (a): density plot, the black oval represents the point of interest, (b): phase plot, the black circle shows the equilibrium point, (c): BSA displacement spectrum, (d): beam 1 displacement spectrum.

dB below that of the second mode. For the results presented in Fig. 15, the BSA is active (allowing an overall attenuation of the frequency response of the linear system of more than 10 dB) with a chaotic motion around its two equilibrium positions. Here again, the spreading of the energy over the whole spectrum has allowed a re-excitation of both the low and high frequency modes of the linear system. For this case also, the peak level of the first mode of the linear system has remained at least 10 to 15 dB below that of the main peak.

To keep a paper length acceptable, only one typical numerical results is given in Fig. 16. It correspond to an excitation close to the linear resonance frequency of the linear system first mode at an amplitude for which the BSA was activated (allowing an overall attenuation of the frequency response of the linear system of more than 15 dB) with a chaotic motion around its two equilibrium positions.

The results presented in Fig. 11, 12, 14 and 15 show a chaotic-like behaviour. To characterize it, the first Lyapunov exponent was computed for all the data [17, 18] using the TISEAN package [19]. The results are given in Tab. 1. In this table, q_e represents the measured BSA displacement, v_e the measured BSA velocity, u_{e1} the measured beam 1 displacement and u_{e2} the measured beam 2 displacement. For all data, the embedding delay τ, the minimal embedding dimension m and the measure for determinism κ are given. τ was estimated by a mutual information routine and is given in sample unit (let us recall that here a sampling rate of 4096 Hz had been chosen). The

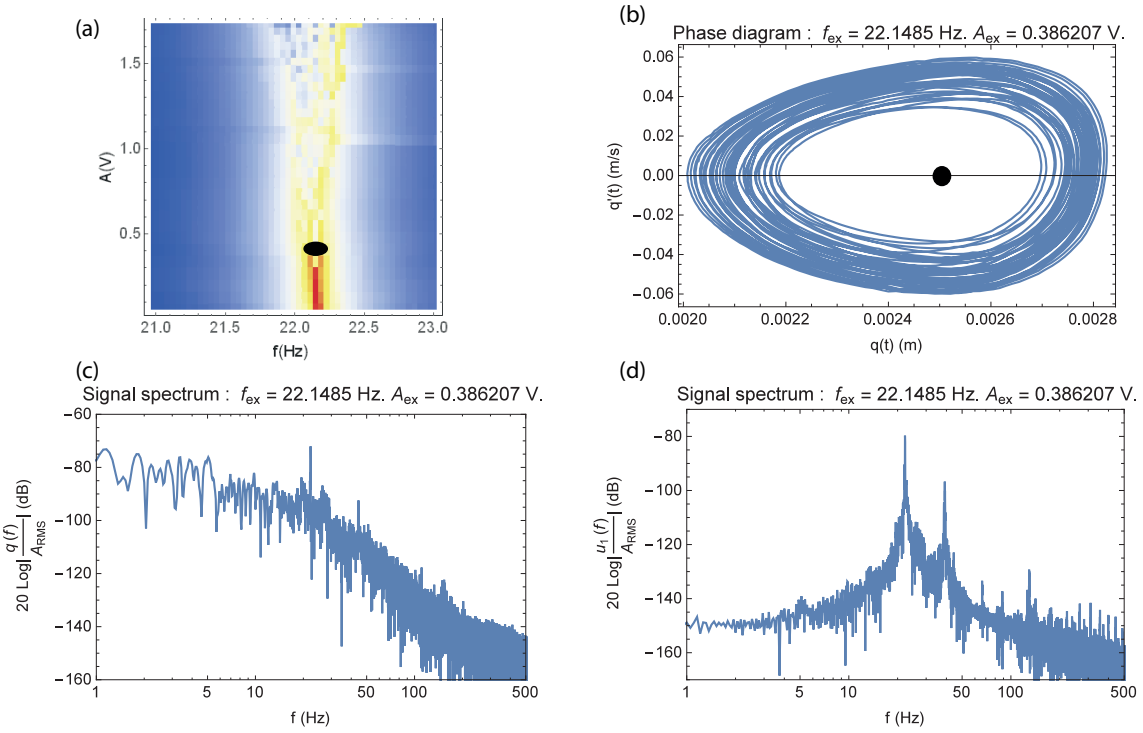

Figure 11: Typical measured system response around the linear system first mode at an excitation frequency $f_{ex} \approx$ 22.15 Hz and amplitude $A_{ex} \approx 0.39$ V. (a): density plot, the black oval represents the point of interest, (b): phase plot, the black circle shows the equilibrium point,(c): BSA displacement spectrum, (d): beam 1 displacement spectrum.

minimal embedding dimension m was obtained by the dimension at with the fraction of false nearest neighbour drops to zero. The measure for determinism allows to distinguish between deterministic chaos and irregular random behaviour. The determinism factor $\kappa \in [0, 1]$ is such as for a perfectly deterministic system κ approaches 1 while for a system with stochastic component κ will be significantly smaller than 1. Finally, the maximal Lyapunov exponent λ_1 was estimated using the Kantz algorithm.

These results reveal interesting features. As expected for a signal with strong periodic component, the embedding delays for all beam displacements correspond roughly to a quarter period of the forcing signal, for example in Fig. 11, for which the excitation frequency $f_{ex} \approx 22.15$ one obtain $\tau \approx 45$ samples, that is $\tau \approx 4096/(4 \times 22.5)$. The significant BSA embedding delay change observed for the data in Fig. 12 and Fig. 15 reveals that the forcing signal remains no longer visible in the BSA (this is confirmed by the spectra for these two configurations) indicating a dramatic change in the response of the BSA. This is not the case for the numerical results given in Fig. 15 for which the embedding delay stay close to a quarter period of the forcing signal; in that case, the BSA spectrum reveals the presence of the forcing signal. For all the measurements, the determinism factor κ stays sufficiently close to 1 to validate the signature for a deterministic chaos.

The main feature that emerges from the results given in Tab. 1 is that every set of data,

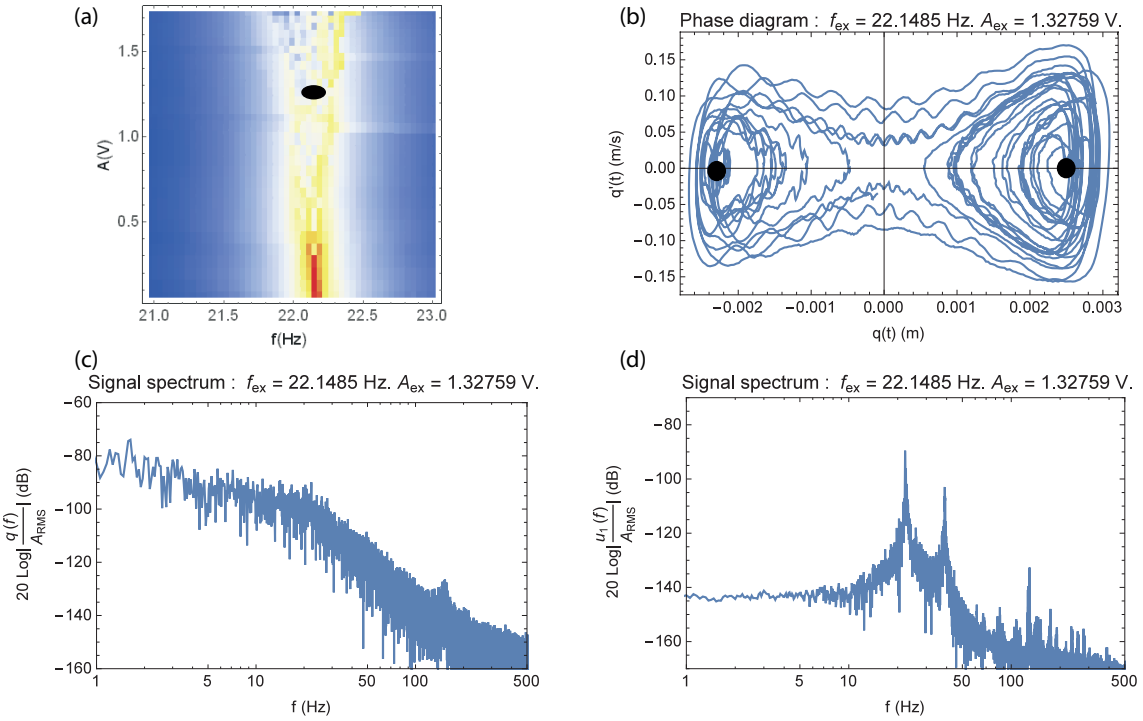

Figure 12: Typical measured system response around the linear system first mode at an excitation frequency $f_{ex} \approx$ 22.15 Hz and amplitude $A_{ex} \approx 1.33$ V. (a): density plot, the black oval represents the point of interest, (b): phase plot, the black circles show the equilibrium points,(c): BSA displacement spectrum, (d): beam 1 displacement spectrum.

experimental or numerical, possess a positive Lyapunov exponent. It is small and of same order for all data for the results presented in Fig. 11 and 14 indicating the start of chaotic motion for the BSA. It becomes large for the experimental results presented in Fig.12 and in Fig.15 and for the numerical result presented in Fig. 16, indicating a deterministic chaotic motion of the BSA. It these cases, even if the beam motions are dominated by the forcing signal, a trace of the strong chaotic motion of the BSA remains visible on their movements.

4.2. Attenuation of the FRF around the first two modes: brief parametric study

An example of parametric study is given in Fig. 17 and 18 for the first mode and in Fig. 19 and 20 for the second mode to evaluate the influence of the damping of the BSA. The linear resonance of the BSA remains fixed at 29 Hz, with damping fixed at $\mu = 0.05$ kg/s and $\mu = 0.15$ kg/s in Fig. 17 and 19 and $\mu = 0.35$ kg/s and $\mu = 0.50$ kg/s in Fig. 18 and 20, with all other parameters of the system remaining fixed. Each curve is obtained within 10 minutes of computation on a four cores workstation using Mathematica's parallelization ability [15]. It is worth noting that the FRF reference level of linear system has decreased with increasing damping indicating that the overall damping was significantly influenced by the BSA damping. These results show that, in the present case, when the damping of the BSA is of the same order than that of the primary system (let us

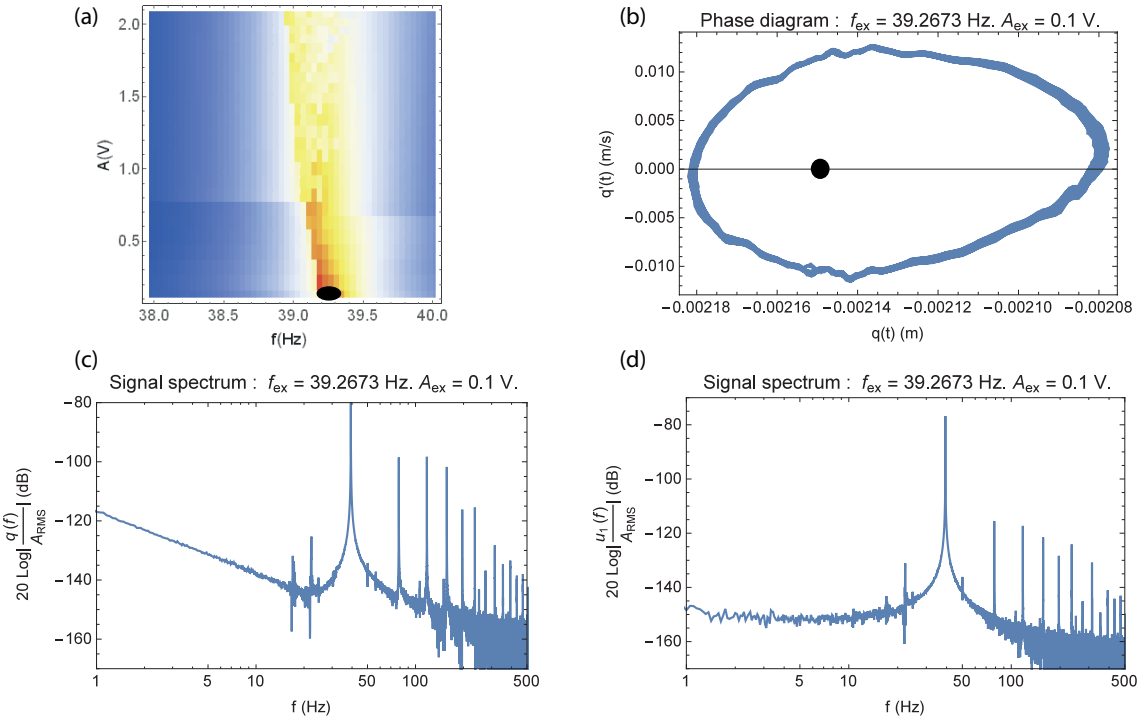

Figure 13: Typical measured system response around the linear system second mode at an excitation frequency fex ≈ 39.27 Hz and amplitude Aex ≈ 0.1 V. (a): density plot, the black oval represents the point of interest, (b): phase plot, the black circle shows the equilibrium point, (c): BSA displacement spectrum, (d): beam 1 displacement spectrum.

recall that each beam has a viscous damping $\mu_b = 0.1$ kg/s), its variation has not a great influence on the observed attenuation.

The second example of parametric study is obtained by varying the linear resonance of the BSA while fixing its damping to $\mu = 0.24$ kg/s. But in that case, care must be taken to avoid a linear resonance close to one of the primary system (ie 22 Hz and 38 Hz) because in that case, the BSA acts as a tuned mass damper. As shown by Den Hartog [2], for a small mass linear absorber, with $\overline{m} = m_N/m_1 \approx 0.005 \ll 1$, for each resonance of the primary system $\check{f}_i, i = 1, 2$, an optimal tuned mass damped (TMD) would have a linear resonance $f_i^{opt} = \check{f}_i\sqrt{1 - 0.5\overline{m}}/(1 + \overline{m}) \approx \check{f}_i, i = 1, 2$. Four computed different linear frequency responses of the beam 1 of the 3-dof linear system for different linear resonances of the BSA acting as a linear mass damper are presented in Fig. 21; in this figure, the maximum frequency response around each resonance had been spotted on the y-axis. As stated, when the resonance of the BSA acting as a linear absorber is tuned to the resonance of the primary system, a significant attenuation is obtained. And, as showed by Vigui and Kerschen [20], this maximum attenuation corresponds more or less to a limit of attenuation for BSA.

Two frequencies of the linear resonance of the BSA are shown: $\check{f}_N \approx 17$ Hz in Fig. 22, below the first resonance of the primary system and$\check{f}_N \approx 48$ Hz in Fig. 23, above its second resonance. In each figure, the two horizontal lines correspond to the frequency response obtained for the linear

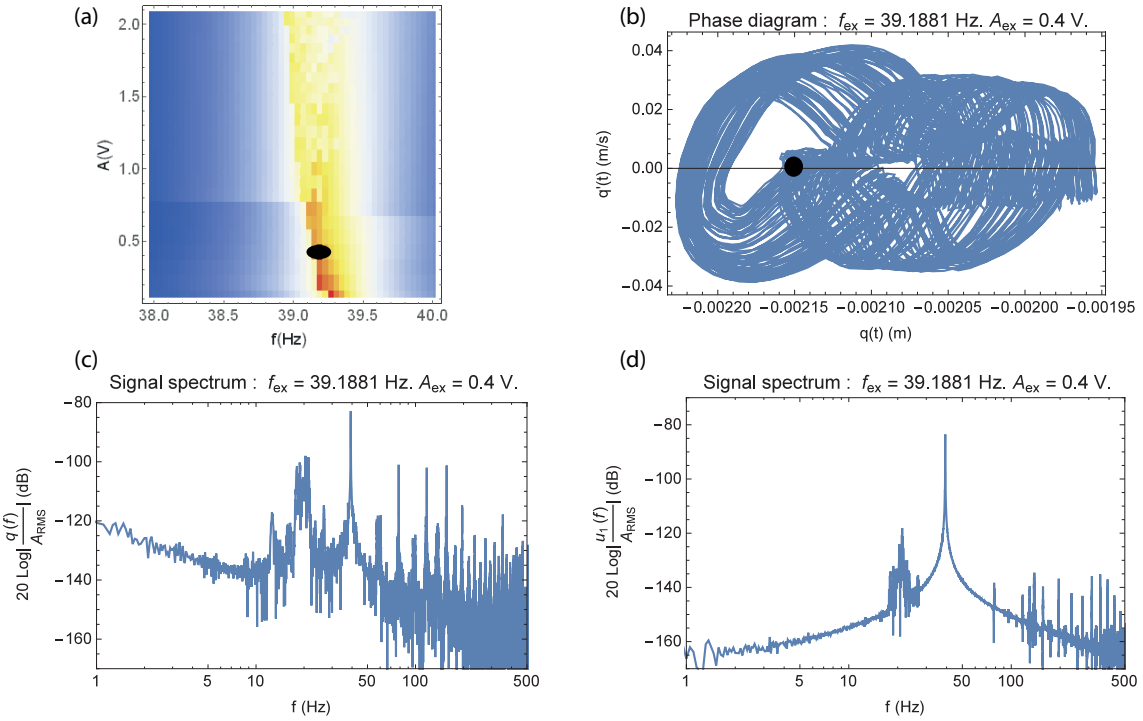

Figure 14: Typical measured system response around the linear system second mode at an excitation frequency fex ≈ 39.19 Hz and amplitude Aex ≈ 0.4 V. (a): density plot, the black oval represents the point of interest, (b): phase plot, the black circle shows the equilibrium point, (c): BSA displacement spectrum, (d): beam 1 displacement spectrum.

mass damper: one for the linear resonance of the BSA and one for the linear resonance of the TMD. It is worth noting, as observed by Vigui and Kerschen [20] that the efficiency of the BSA tends to that of the TMD without reaching it. As previously observed [21], if a better attenuation around a particular mode can be obtained by a fine tuning of the characteristics of the BSA (linear resonance and damping), it deteriorates the other. For example, the best attenuation (up to 20 dB) for the second mode is observed for a BSA linear resonance $\check{f}_N \approx 48$ Hz as shown in the right curve of Fig. 23 but in that case, instead of up to 18 dB attenuation around the first mode as observed in the left curve of Fig. 18, obtained for a linear resonance $\check{f}_N \approx 29$ Hz, the attenuation around the first mode is limited up to 10 dB, as shown in the right curve of Fig. 22. In the case considered here, the BSA damping must be of the same order than that of the primary system alone and its linear resonance must be chosen between those of the two modes to control.

5. Conclusion

In this paper, a linear system formed by two coupled linear Euler vibrating beams around its two first modes coupled to a bistable NES has been experimentally and numerically studied. The bistable NES was made by attaching a small mass at the center of a very thin buckled beam fixed on an ABS support. Using Ritz procedure, a simplified three degrees of freedom model has been

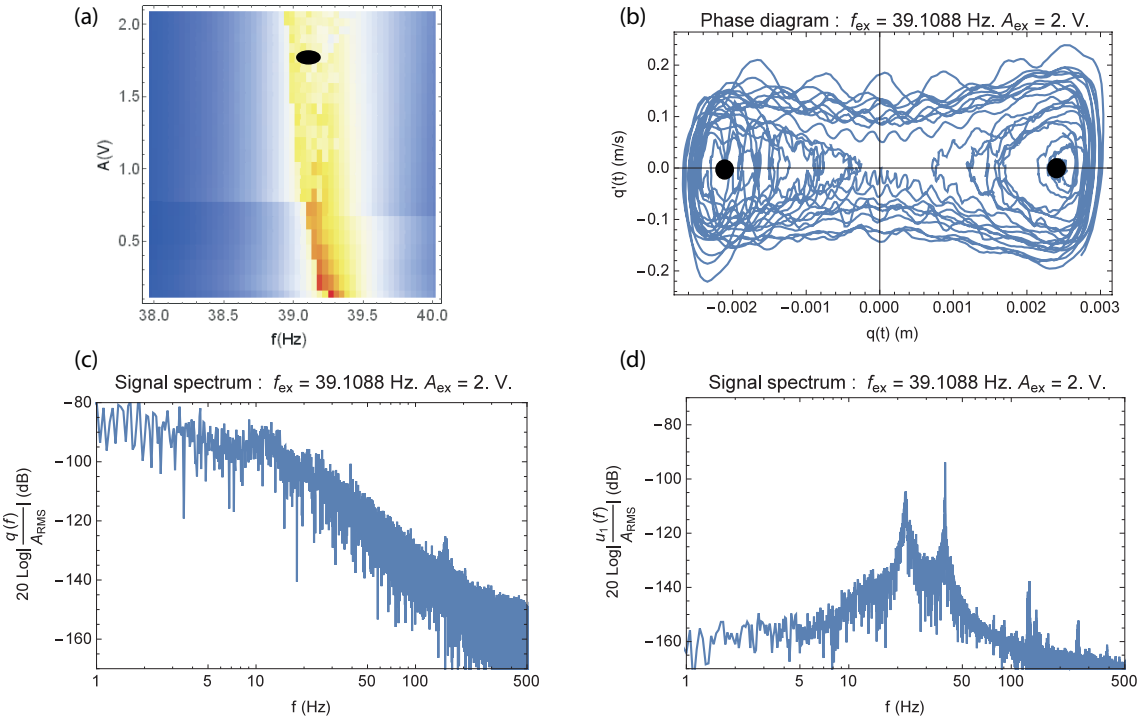

Figure 15: Typical measured system response around the linear system second mode at an excitation frequency $f_{ex} \approx 39.11$ Hz and amplitude $A_{ex} \approx 2$ V. (a): density plot, the black oval represents the point of interest, (b): phase plot, the black circles show the equilibrium points, (c): BSA displacement spectrum, (d): beam 1 displacement spectrum.

developed to describe both linear, using the first mode of a cantilever beams, and nonlinear parts of the complete system. The bistable NES, using the Ritz procedure with the first mode of a fixed buckled beam, has been described by a viscous one degree of freedom Helmholtz-Duffing nonlinear differential equation. The stiffness and damping parameters of this nonlinear equation had been adjusted to fit the measured linear mode of the buckled beam.

The results presented here, both experimental and numerical, show that a very simple nonlinear bi-stable NES is able to strongly reduce the amplitude of a primary system with multiple resonance. Without any particular optimisation, a reduction up to 10 dB of the vibration amplitude level of primary linear system was experimentally observed. It was observed that most of the energy reduction of the primary system was attained when the dynamics of the bistable NES was a chaotic motion around its two equilibrium positions. In that case, the spreading the energy over the whole spectrum has allowed a re-excitation of both the low and high frequency modes of the linear system but at a level at least 10 to 15 dB below that of the main mode.

The parametric study conducted on the simple model describing the system reveals that this result, not only can easily be obtained for a large class of configuration of the nonlinear bi-stable NES but also that under particular conditions, an even stronger attenuation is possible. It is worth noting that the weight of the nonlinear bi-stable NES was small compared to the primary system weighing 500 g since the weight of the nonlinear bi-stable NES itself was less than 3 g and that of

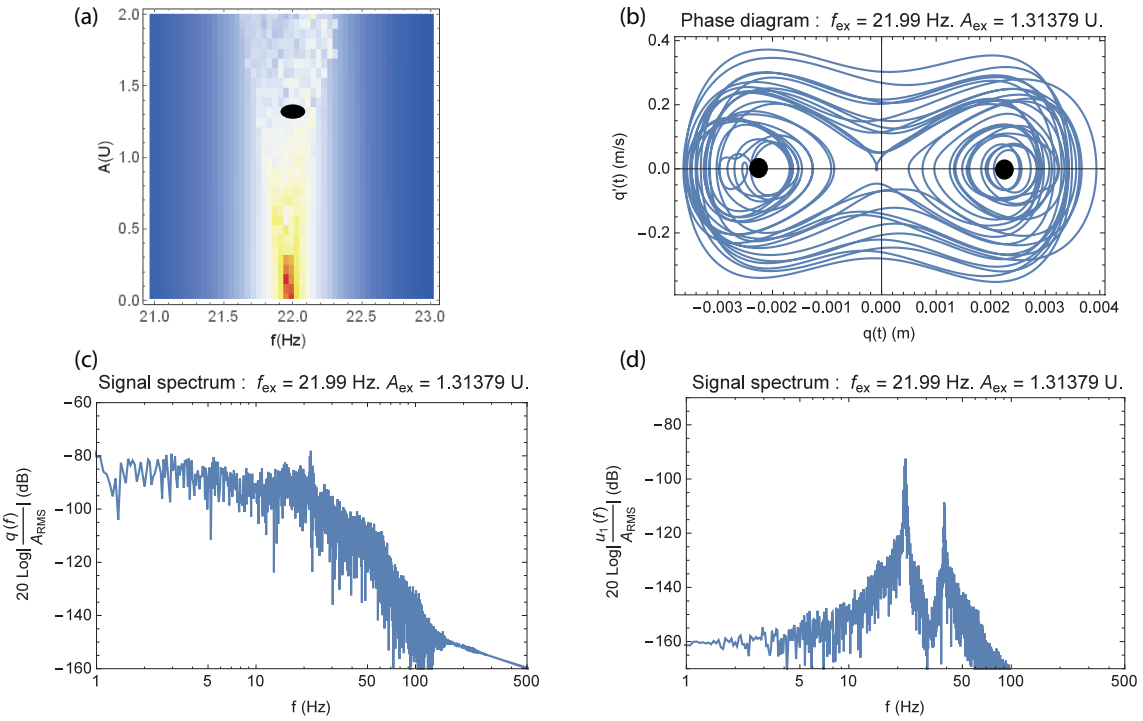

Figure 16: Typical calculated system response around the linear system first mode at an excitation frequency $f_{ex} \approx 22$ Hz and amplitude $A_{ex} \approx 1.31$ U. (a): density plot, the black oval represents the point of interest, (b): phase plot, the black circles show the equilibrium points, (c): BSA displacement spectrum, (d): beam 1 displacement spectrum.

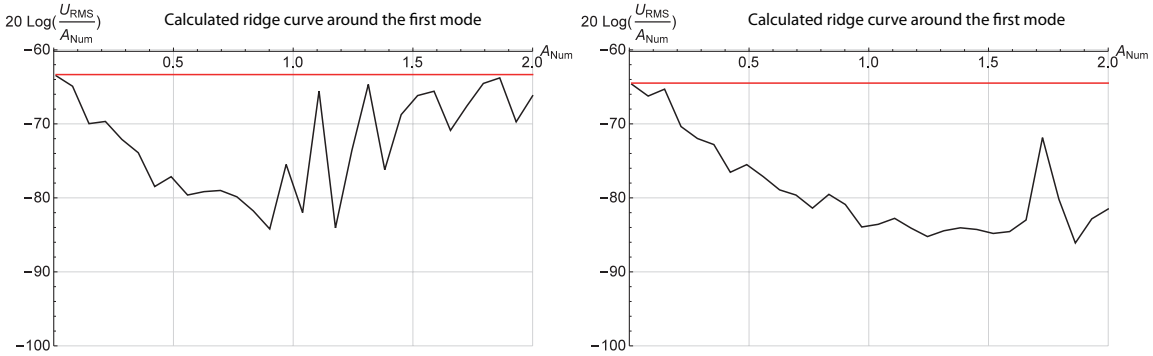

Figure 17: Calculated ridge curve of beam 1 displacement frequency response around the first mode for different BSA damping. Left: viscous damping $\mu = 0.05$ kg/s, right: viscous damping $\mu = 0.15$ kg/s. The straight line corresponds to the ridge curve for the linear BSA.

the support was about 30 g. Our recent experiments, still in progress, made on a thin plate excited by acoustic sound waves show a similar ability. These various results have confirmed the very interesting feature of this nonlinear bi-stable NES, that is contrarily to the usual NES (generally a

	q_e	v_e	u_{e1}	u_{e2}
Fig. 11	$\tau = 45$ $m = 8$ $\kappa = 0.97$ $\lambda_1 = 0.12$	$\tau = 42$ $m = 9$ $\kappa = 0.88$ $\lambda_1 = 0.12$	$\tau = 45$ $m = 8$ $\kappa = 0.96$ $\lambda_1 = 0.10$	$\tau = 45$ $m = 8$ $\kappa = 0.93$ $\lambda_1 = 0.08$
Fig. 12	$\tau = 136$ $m = 11$ $\kappa = 0.8$ $\lambda_1 = 0.55$	$\tau = 53$ $m = 10$ $\kappa = 0.83$ $\lambda_1 = 1.35$	$\tau = 42$ $m = 8$ $\kappa = 0.97$ $\lambda_1 = 4.5$	$\tau = 42$ $m = 8$ $\kappa = 0.98$ $\lambda_1 = 4.6$
Fig. 14	$\tau = 33$ $m = 10$ $\kappa = 0.93$ $\lambda_1 = 0.25$	$\tau = 29$ $m = 9$ $\kappa = 0.98$ $\lambda_1 = 0.86$	$\tau = 27$ $m = 7$ $\kappa = 0.99$ $\lambda_1 = 0.08$	$\tau = 27$ $m = 8$ $\kappa = 0.98$ $\lambda_1 = 0.14$
Fig. 15	$\tau = 132$ $m = 10$ $\kappa = 0.94$ $\lambda_1 = 3.6$	$\tau = 57$ $m = 10$ $\kappa = 0.82$ $\lambda_1 = 4.4$	$\tau = 31$ $m = 7$ $\kappa = 0.98$ $\lambda_1 = 10.8$	$\tau = 31$ $m = 8$ $\kappa = 0.97$ $\lambda_1 = 8.2$
Fig. 16	$\tau = 46$ $m = 6$ $\kappa = 0.98$ $\lambda_1 = 9.5$	$\tau = 47$ $m = 6$ $\kappa = 0.97$ $\lambda_1 = 9$	$\tau = 44$ $m = 5$ $\kappa = 0.99$ $\lambda_1 = 10.6$	$\tau = 44$ $m = 5$ $\kappa = 0.99$ $\lambda_1 = 10.8$

Table 1: Computation of the first Lyapunov exponent for the experimental (Fig.11, 12, 14 and 15) and numerical data (Fig. 16). q_e: BSA displacement, v_r: BSA velocity, u_{e1}: beam 1 displacement, u_{e2}: beam 2 displacement. τ: estimated embedding delay, m: estimated embedding dimension, κ: measure for determinism, λ_1: First Lyapunov exponent

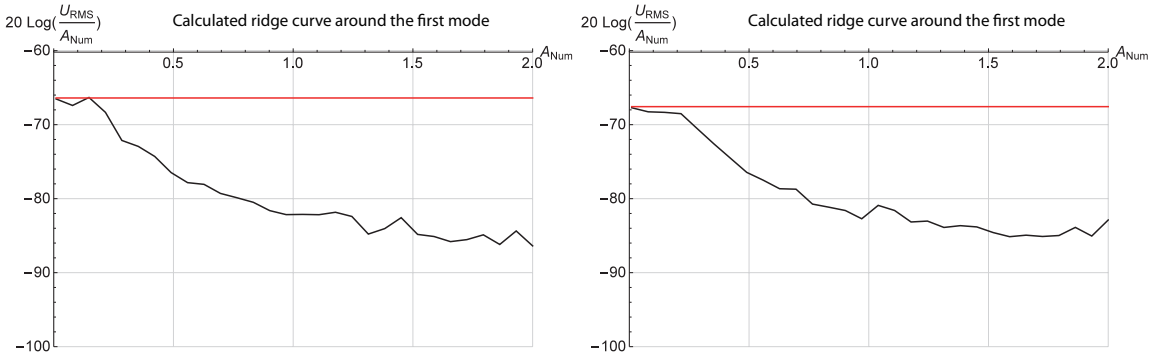

Figure 18: Calculated ridge curve of beam 1 displacement frequency response around the first mode for different BSA damping. Left: viscous damping $\mu = 0.35$ kg/s, right: viscous damping $\mu = 0.50$ kg/s. The straight line corresponds to the ridge curve for the linear BSA.

cubic non linear absorber), the linear frequency of the absorber could be greater than that of the linear system to control. This combined with the unique feature of the bistable NES, as noted by Romeo et al. [11], that is to attain the passive targeted energy transfer at low amplitude, make the bistable NES a very promising way to passive non linear control.

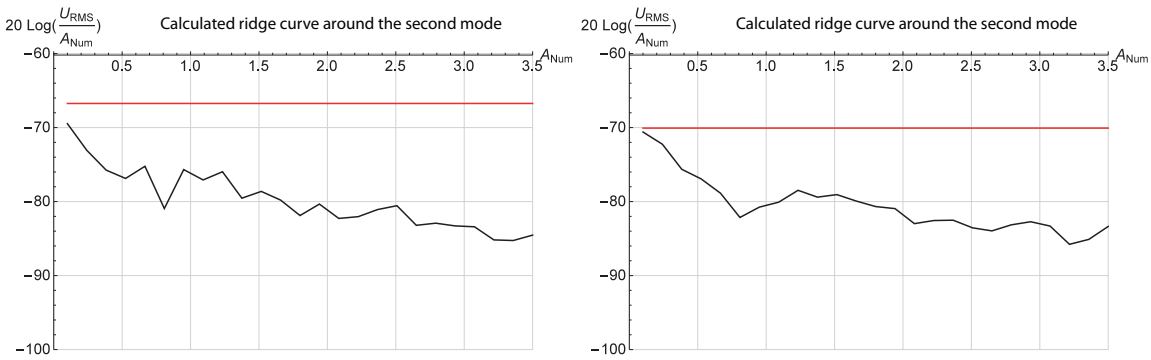

Figure 19: Calculated ridge curve of beam 1 displacement frequency response around the second mode for different BSA damping. Left: viscous damping $\mu = 0.05$ kg/s, right: viscous damping $\mu = 0.15$ kg/s. The straight line corresponds to the ridge curve for the linear BSA.

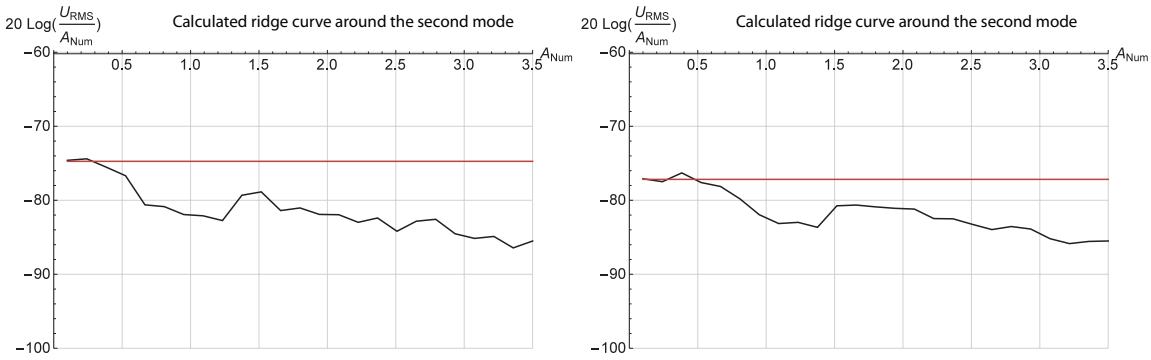

Figure 20: Calculated ridge curve of beam 1 displacement frequency response around the second mode for different BSA damping. Left: viscous damping $\mu = 0.35$ kg/s, right: viscous damping $\mu = 0.50$ kg/s. The straight line corresponds to the ridge curve for the linear BSA.

6. Appendix A. Approximate one degree-of-freedom Helmholtz-Duffing equation for the bistable attachment response.

In this appendix, we present the Ritz method that transforms the equation governing the non linear transverse planar vibration of the BSA with a mass attached at its center into an approximate one degree-of-freedom Helmholtz-Duffing non linear equation.

First of all, it is classical that the equation governing the non linear transverse planar vibration of the clamped-clamped buckled beam whose displacement is $w(x,t)$ is given by (see eg [13] or [14]) :

$$(\rho A + m_0\delta_{\ell/2}(x))\frac{\partial^2 w}{\partial t^2} + EI\frac{\partial^4 w}{\partial x^4} + N\frac{\partial^2 w}{\partial x^2} + \mu\frac{\partial w}{\partial t} - \frac{EA}{2\ell}\frac{\partial^2 w}{\partial x^2}\int_0^\ell (\frac{\partial w}{\partial x})^2\,\mathrm{d}x = F(x)H_t(t)\cos(\omega t), \quad (11)$$

with $I = eh^3/12$ and $A = eh$. $\delta_{\ell/2}(x)$ is the Dirac delta distribution located at the center of the BSA. $H_t(t)$ is the Heaviside unit step function that is equal to zero if $t < 0$ and equal to one if

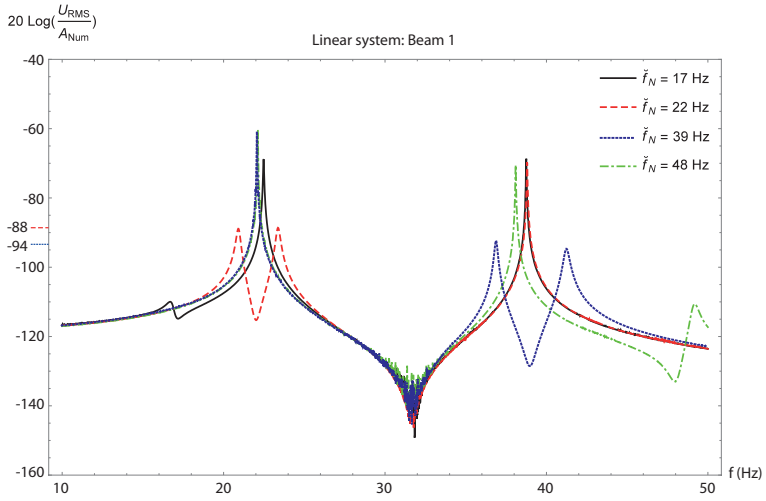

Figure 21: Four computed beam 1 different linear frequency responses. Each curve corresponds to the BSA acting as a linear absorber with a particular resonance frequency: 17 Hz, 22 Hz (TMD for the first mode), 39 Hz (TMD for the second mode) and 48 Hz and viscous damping $\mu = 0.24$ kg/s.

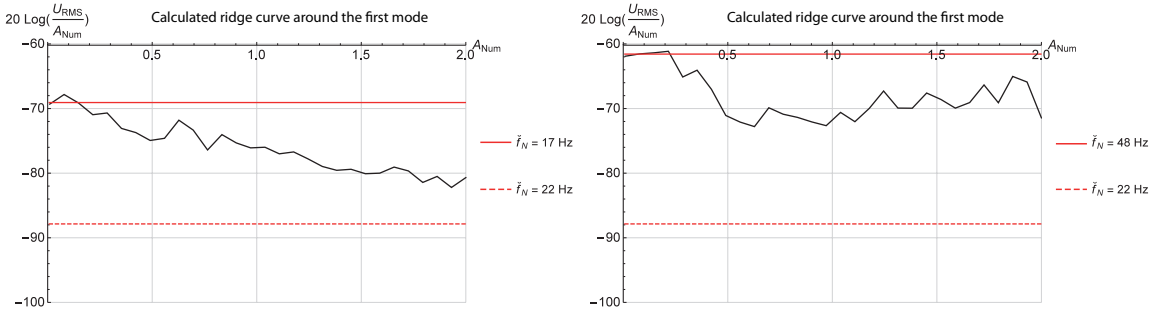

Figure 22: Calculated ridge curve of beam 1 displacement frequency response around the first mode for different BSA linear resonance. Left: $\check{f}_N \approx 17$ Hz, right: $\check{f}_N \approx 48$ Hz. The two horizontal lines correspond to the frequency response curve for the linear BSA: the continuous one is for the BSA frequency used in the non linear response while the discontinuous is the one obtained for the TMD.

$t \geq 0$. To this equation, one adds the initial conditions $w(x, t = 0) = 0$ and $\partial w/\partial t(x, t = 0) = 0$ and the usual boundary conditions for a clamped beam given by :

$$\begin{cases} w = 0, \frac{\partial w}{\partial x} = 0 \text{ at } x = 0, \\ w = 0, \frac{\partial w}{\partial x} = 0 \text{ at } x = \ell. \end{cases} \tag{12}$$

One defines the non dimensional quantities as $\tilde{x} = x/\ell$, $\tilde{w} = w/r$ where $r = \sqrt{I/A}$ is the radius of gyration of the cross section, $\omega_0 = 1/\ell^2\sqrt{EI/(\rho A)}$, $\tilde{t} = \omega_0 t$, $\tilde{\omega} = \omega/\omega_0$, $\tilde{N} = N\ell^2/(EI)$. Let us denote $\tilde{N}_c = 4\pi^2$ the non dimensional critical load, one defines $\tilde{b} = b/r = \sqrt{4(N - N_c)/\pi^2}$ as the non-dimensional post buckling deflection. The non dimensional displacement of the clamped

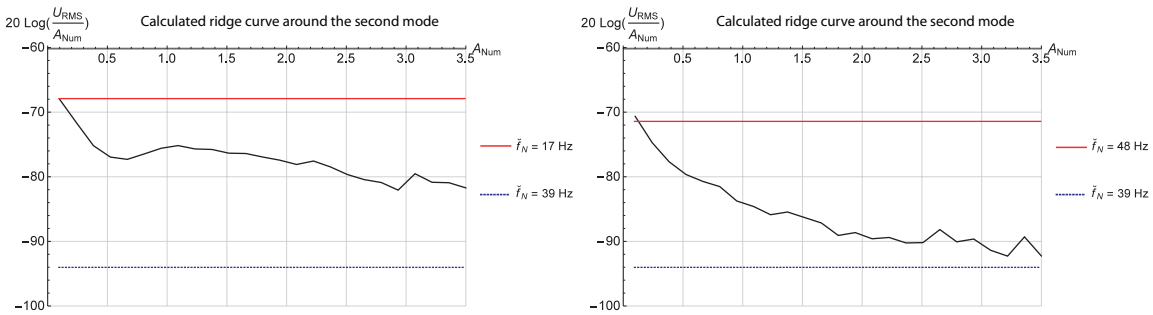

Figure 23: Calculated ridge curve of beam 1 displacement frequency response around the second mode for different BSA linear resonance. Left: $\check{f}_N \approx 17$ Hz, right: $\check{f}_N \approx 48$ Hz. The two horizontal lines correspond to the frequency response curve for the linear BSA: the continuous one is for the BSA frequency used in the non linear response while the discontinuous is the one obtained for the TMD.

buckled beam is written as

$$\tilde{w}(\tilde{x},\tilde{t}) = \tilde{w}_0(\tilde{x}) + \tilde{v}(\tilde{x},\tilde{t}), \text{ with } \tilde{w}_0(\tilde{x}) = \frac{1}{2}\tilde{b}(1-\cos 2\pi\tilde{x}). \tag{13}$$

$\tilde{w}_0(\tilde{x})$ is the statics buckled configuration [14], solution of the non linear integrodifferential problem

$$\frac{\mathrm{d}^4\tilde{w}_0}{\mathrm{d}\tilde{x}^4} + \left(\tilde{N} - \frac{1}{2}\int_0^1 \left(\frac{\mathrm{d}\tilde{w}_0}{\mathrm{d}\tilde{x}}\right)^2 \mathrm{d}\tilde{x}\right)\frac{\mathrm{d}^2\tilde{w}_0}{\mathrm{d}\tilde{x}^2} = 0, \tag{14}$$

$$\tilde{w}_0 = 0 \text{ and } \frac{\mathrm{d}\tilde{w}_0}{\mathrm{d}\tilde{x}} = 0, \text{ at } \tilde{x} = 0 \text{ and } \tilde{x} = 1. \tag{15}$$

Writing Eq. (11) with non dimensional variables, noting that $\delta_{\ell/2}(x/\ell) = 1/\ell\delta_{1/2}(x/\ell)$, substituting Eq. (13) in Eq. (11) and using Eq. (14) leads to the non linear equation that governs the dynamics of the BSA :

$$(1+\beta\delta_{1/2})\frac{\partial^2\tilde{v}}{\partial\tilde{t}^2} + \frac{\partial^4\tilde{v}}{\partial\tilde{x}^4} + 4\pi^2\frac{\partial^2\tilde{v}}{\partial\tilde{x}^2} - 2\tilde{b}^2\pi^3\cos 2\pi\tilde{x}\int_0^1\frac{\partial\tilde{v}}{\partial\tilde{x}}\mathrm{d}\tilde{x} - \tilde{b}\pi^2\cos 2\pi\tilde{x}\int_0^1(\frac{\partial\tilde{v}}{\partial\tilde{x}})^2\mathrm{d}\tilde{x} =$$
$$+\tilde{b}\pi\frac{\partial^2\tilde{v}}{\partial\bar{x}^2}\int_0^1\frac{\partial\tilde{v}}{\partial\tilde{x}}\sin 2\pi\tilde{x}\mathrm{d}\tilde{x} + \frac{1}{2}(\frac{\partial\tilde{\tilde{v}}}{\partial\tilde{x}})^2\mathrm{d}\tilde{x} - \tilde{\mu}\frac{\partial\tilde{v}}{\partial\tilde{t}} + \tilde{F}(\tilde{x})H_{\tilde{t}}(\tilde{t})\cos(\tilde{\omega}\tilde{t}), \tag{16}$$

together with the initial and boundary conditions. The non dimensional quantities are defined as $\beta = \frac{m_0}{\rho A\ell} \approx 7$ is the ratio of the small mass m_0 to the BSA beam mass, $\tilde{\mu} = \frac{\mu}{\rho A\omega_0}$ is the non-dimensional viscous damping and $\tilde{F}(\tilde{x}) = \frac{\ell^4}{rEI}F(x/\ell)$.

Now let us approximate the dynamic deflection around equilibrium position $\tilde{v}(\tilde{x},\tilde{t})$ using only the first buckling mode as

$$\tilde{v}(\tilde{x},\tilde{t}) = \tilde{w}_0(\tilde{x})\tilde{q}(\tilde{t}). \tag{17}$$

This approximation allows us to describe the change of equilibrium position but does not give access to a fine description of the buckled beam movement [13], particularly near its linear resonance. After introducing Eq. (17) in Eq. (16), a Ritz reduction, ie multiplying both member of Eq. (16)

by $\tilde{w}_0(\tilde{x})$ and integrating both member of the resulting equation on the beam length ℓ, leads to a Helmholtz-Duffing nonlinear equation for the BSA displacement

$$(3/8+\beta)\ddot{\tilde{q}}(\tilde{t})+\frac{3}{8}\tilde{\mu}\dot{\tilde{q}}(\tilde{t})+\frac{\tilde{b}^2\pi^4}{4}\left(\tilde{q}(\tilde{t})+\frac{3}{2}\tilde{q}(\tilde{t})^2+\frac{1}{2}\tilde{q}(\tilde{t})^3\right)=\frac{1}{\tilde{b}^2}H_{\tilde{t}}(\tilde{t})\cos(\tilde{\omega}\tilde{t})\int_0^1\tilde{F}(\tilde{x})\tilde{w}_0(\tilde{x})\mathrm{d}\tilde{x} \quad (18)$$

7. Appendix B. Experimental and numerical examples of the bistable attachment response

In this appendix, we present results for some chosen experimental amplitude-frequency pairs and their corresponding computed pairs for the BSA alone. Each of these plots is composed of four sub-plots : the (a) plot shows the location of the point of interest in the density plot (corresponding to an upside view of the frequency response of the RMS value for the measured or computed BSA displacement given in Fig. 4) as a black oval, the (b) plot shows the spectrum of the signal, the (c) curve is a phase plot (displacement/velocity) for one second recorded (or computed) signal and the (d) shows the time signal of the displacement. As the mounting of the BSA on the shaker does not allow a simultaneous measurement of velocity and displacement, the displacement was estimated from velocity measurements by numerical integration. The change of equilibrium positions make the integration constants difficult to estimate; while correct in amplitude, the sign of the displacement value has little signification. To see it, it had been reported on the various phase plots the equilibrium positions as black circles. Since the model differs from the experiment, instead of looking for strict correspondence at amplitude-frequency pairs, we propose to find a correspondence between pairs located near zones of interest.

The first zone is located close to the half linear resonance of the BSA at low amplitude. We present in Fig. 24 the measured signal and in Fig. 25 the computed signal. In these low amplitude and frequency ranges, the model is able to describe very precisely most of the features observed experimentally (amplitude, phase portrait and spectrum).

The second zone is located close to the non linear resonance of the BSA at medium excitation amplitude at the beginning of the high amplitude movements of the BSA with chaotic motion. We present in Fig. 26 the measured signal and in Fig. 27 the computed signal. These curves reveal the main limitation of our simplified model. For this chaotic motion, it appears that our one degree of freedom viscous model is not able to describe finely all the features of the experiment. Here, the computed amplitude is clearly overestimated by a factor two. But as shown by the results, this not a real problem since the important feature here is the chaotic motion of the BSA that spreads the energy over the a large spectrum. When connected to the linear system, this energy re-repartition over the spectrum acts like a dissipation of the energy since the primary linear system to control not only responds at its resonances, but also dissipates energy by viscosity.

This is confirmed by the observation of the third zone, that is located above the linear resonance of the BSA at high excitation amplitude showing a high amplitude chaotic movements zone of the BSA. We present in Fig. 28 the measured signal and in Fig. 29 the computed signal. There is always an overestimation of the amplitude of the BSA displacement but on the whole, the chaotic motion is well described.

[1] H. Frahm, Device for Damping Vibrations of Bodies, U.S. Patent No. 989,958, 1909.

[2] J.P. Den Hartog, Mechanical Vibration, McGraw-Hill, New York, 1947.

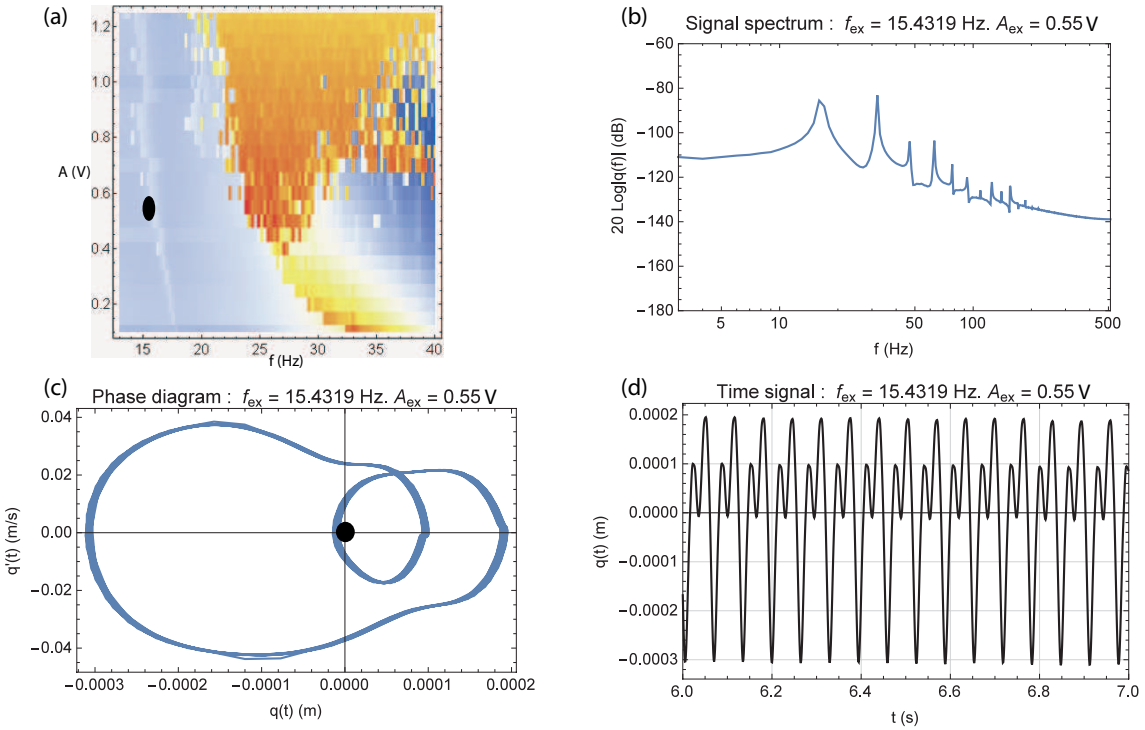

Figure 24: Measured BSA response. (a): density plot, the black oval represents the point of interest, (b): displacement spectrum, (c): phase plot, the black circle shows the equilibrium point, (d): displacement time recording.

[3] O. Gendelman, L.I. Manevitch, A.F. Vakakis, R.M. Closkey, Energy Pumping in Nonlinear Mechanical Oscillators: Part I–Dynamics of the underlying Hamiltonian systems. ASME Journal of Applied Mechanics 68 (2011) 34-42. doi:10.1115/1.1345524

[4] A.F. Vakakis, O.V. Gendelman, Energy Pumping in Nonlinear Mechanical Oscillators: Part II–Resonance Capture. ASME Journal of Applied Mechanics 68 (2011) 42-48. doi:10.1115/1.1345525

[5] A.F. Vakakis, O.V. Gendelman, L.A. Bergman, D.M. McFarland, G. Kerschen, Y.S. Lee, Nonlinear Targeted Energy Transfer in Mechanical and Structural Systems (two volumes). Springer Verlag, Berlin, 2008. doi:10.1007/978-1-4020-9130-8

[6] R. Bellet, B. Cochelin, R. Côte, P.-O. Mattei, Enhancing the dynamic range of targeted energy transfer in acoustics using several nonlinear membrane absorbers. Journal of Sound and Vibration 331 (2012) 5657-5668. doi:10.1016/j.jsv.2012.07.013

[7] R. Mariani, S. Bellizzi, B. Cochelin, Ph. Herzog, P.-O. Mattei, Toward an adjustable non linear low frequency acoustic absorber. Journal of Sound and Vibration 330 (2012) 5245-5258. doi:10.1016/j.jsv.2011.03.034

[8] E. Gourdon, C.H. Lamarque, Energy Pumping with Various Nonlinear Structures: Numerical Evidences. Nonlinear Dynamics, 40 (2005) 281-307. doi: 10.1007/s11071-005-6610-6

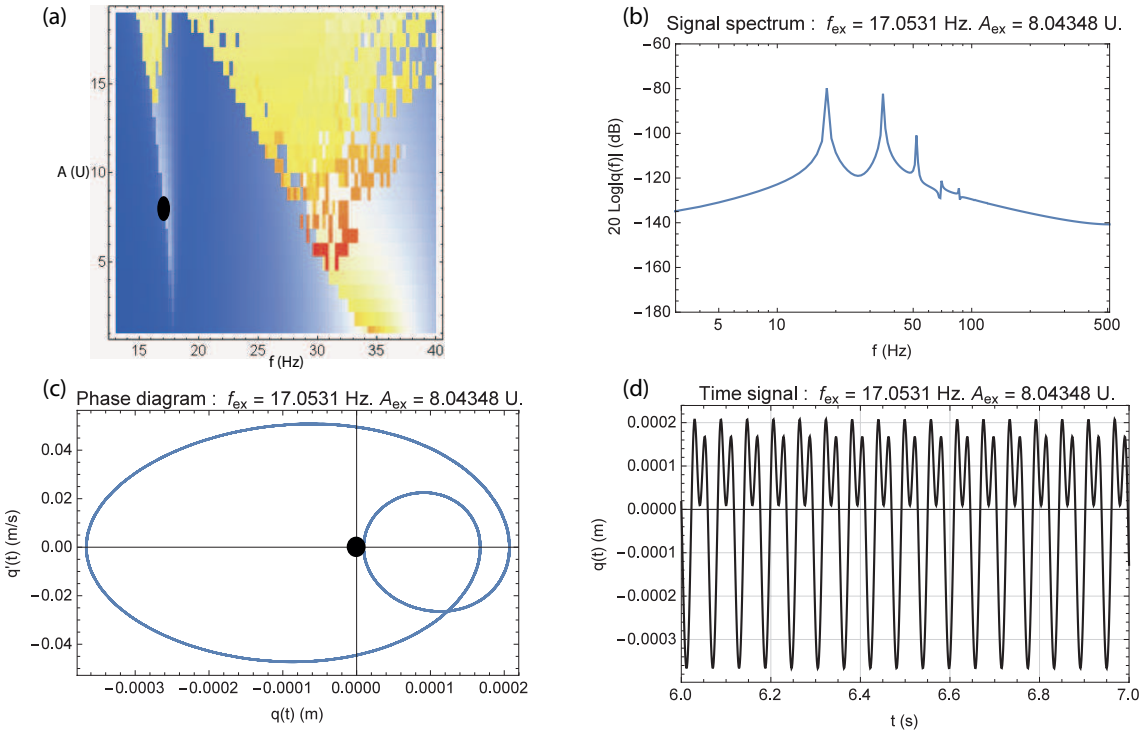

Figure 25: Computed BSA response. (a): density plot, the black oval represents the point of interest, (b): displacement spectrum, (c): phase plot, the black circle shows the equilibrium point, (d): displacement time recording.

[9] A. Ture Savadkoohi, L.I. Manevitch, C.H. Lamarque, Analysis of the transient behavior in a two dof nonlinear system. Chaos, Solitons & Fractals 44 (2011) 450-463. doi: 10.1013/j.chaos.2011.03.007

[10] L.I. Manevitch, G. Sigalov, F. Romeo, L.A. Bergman, A. Vakakis, Dynamics of a Linear Oscillator Coupled to a Bistable Light Attachment: Analytical Study. ASME Journal of Applied Mechanics 81 (2014) 041011-1-9. doi:10.1115/1.4025150

[11] F. Romeo, L.I. Manevitch, L.A. Bergman, A. Vakakis, Transient and chaotic low-energy transfers in a system with bistable nonlinearity, Chaos 25 (2015) 053109. doi:10.1063/1.4921193

[12] E. Ventsel, Th.Krauthammer, Thin Plates and Shells. Theory, Analysis, and Applications, Marcel Dekker, New York-Basel, 2001.

[13] W. Kreider, A.H. Nayfeh, Experimental Investigation of Single-Mode Response in a Fixed-Fixed Buckled Beam, Nonlinear Dynamics 15 (1998) 155-177. doi:10.1023/A:1008231012968

[14] S. A Emam, A.H. Nayfeh, On the Nonlinear Dynamics of a Buckled Beam Subjected to a Primary-resonance Excitation. Nonlinear Dynamics 35 (2004) 1-17. doi:10.1023/B:NODY.0000017466.71383.d5

[15] Wolfram Mathematica 10, Wolfram Research Inc., Champaign, IL, USA, 2014.

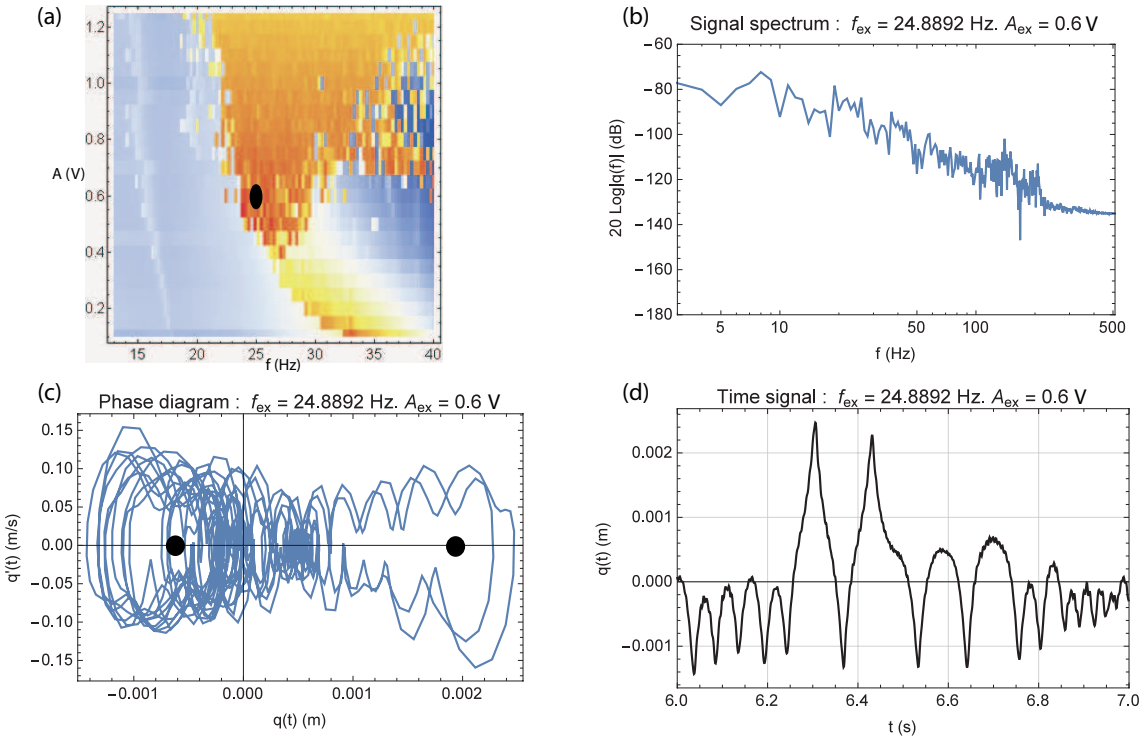

Figure 26: Measured BSA response. (a): density plot, the black oval represents the point of interest, (b): displacement spectrum, (c): phase plot, the black circles show the equilibrium points, (d): displacement time recording.

[16] S.A. Emam, A theoretical and Experimental Study of Nonlinear Dynamics of Buckled Beams, PhD thesis, Virginia Polytechnic Institute and State University, 2002.

[17] H. Kantz; T. Schreiber, Nonlinear Time Series Analysis, Second Edition, Cambridge University Press, Cambridge, 2004.

[18] S. Kodba, M. Perc, M.Marh, Detecting chaos from a time series, European Journal of Physics 26 (2005) 205-215. doi:10.1088/0143-0807/26/1/021

[19] R. Hegger, H. Kantz, T. Schreiber, Practical implementation of nonlinear time series methods: The TISEAN package, Chaos 9 (1999) 413-435. doi: 10.1063/1.166424

[20] R. Vigui, G. Kerschen, Nonlinear vibration absorber coupled to a nonlinear primary system: a tuning methodology. Journal of Sound and Vibration 326 (2009) 780-793. doi:10.1016/j.jsv.2009.05.023

[21] M. Paresh, M. Dardel, M.H. Ghasemi, Performance comparison of nonlinear energy sink and linear tuned mass damper in steady-state dynamics of a linear beam. Nonlinear Dynamics 81 (2015) 1981-2002. doi:10.1007/s11071-015-2120-3

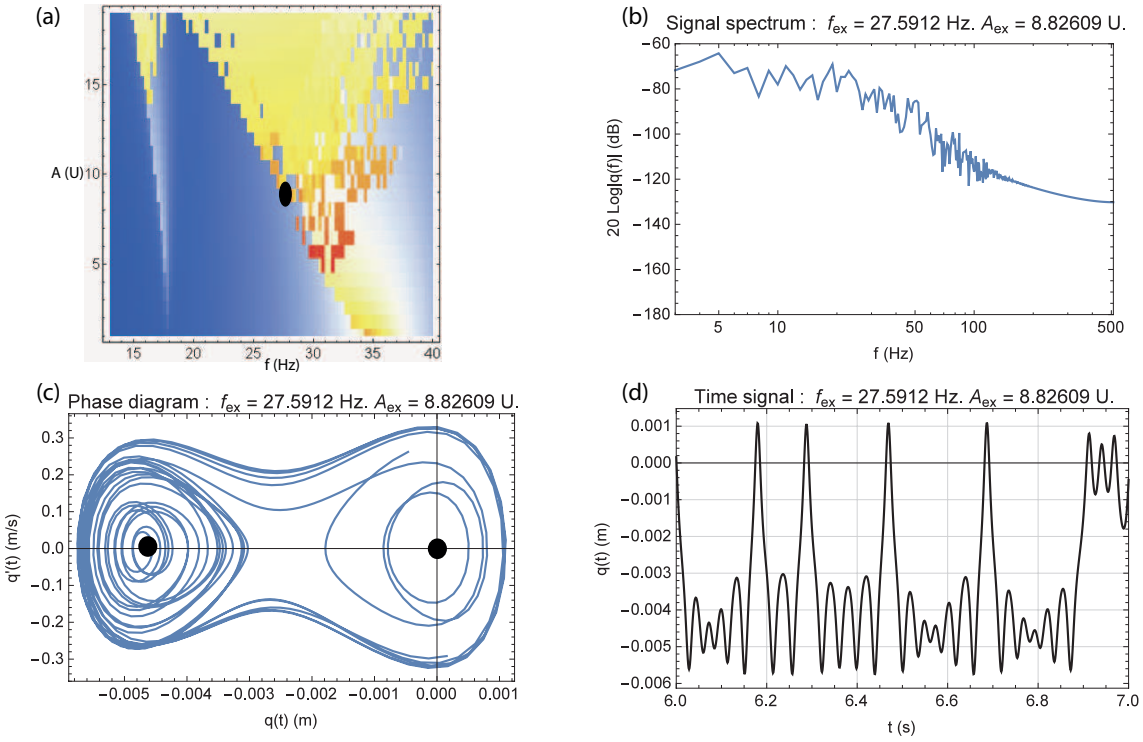

Figure 27: Computed BSA response.(a): density plot, the black oval represents the point of interest, (b): displacement spectrum, (c): phase plot, the black circles show the equilibrium points, (d): displacement time recording.

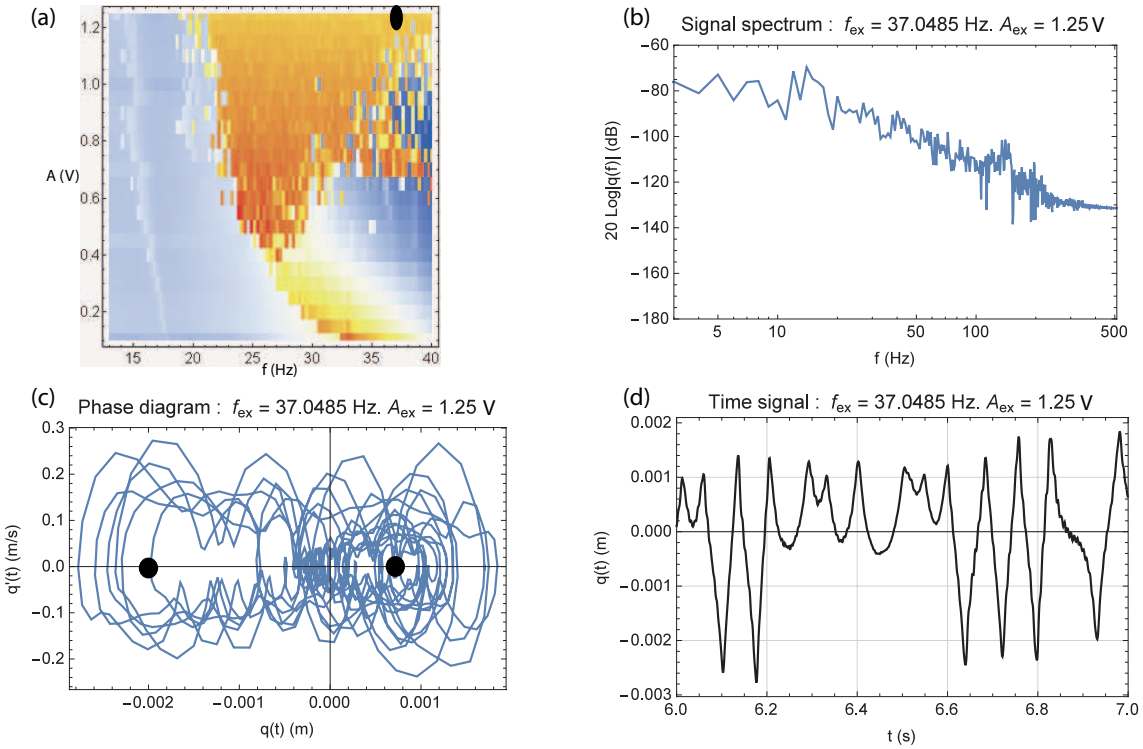

Figure 28: Measured BSA response. (a): density plot, the black oval represents the point of interest, (b): displacement spectrum, (c): phase plot, the black circles show the equilibrium points, (d): displacement time recording.

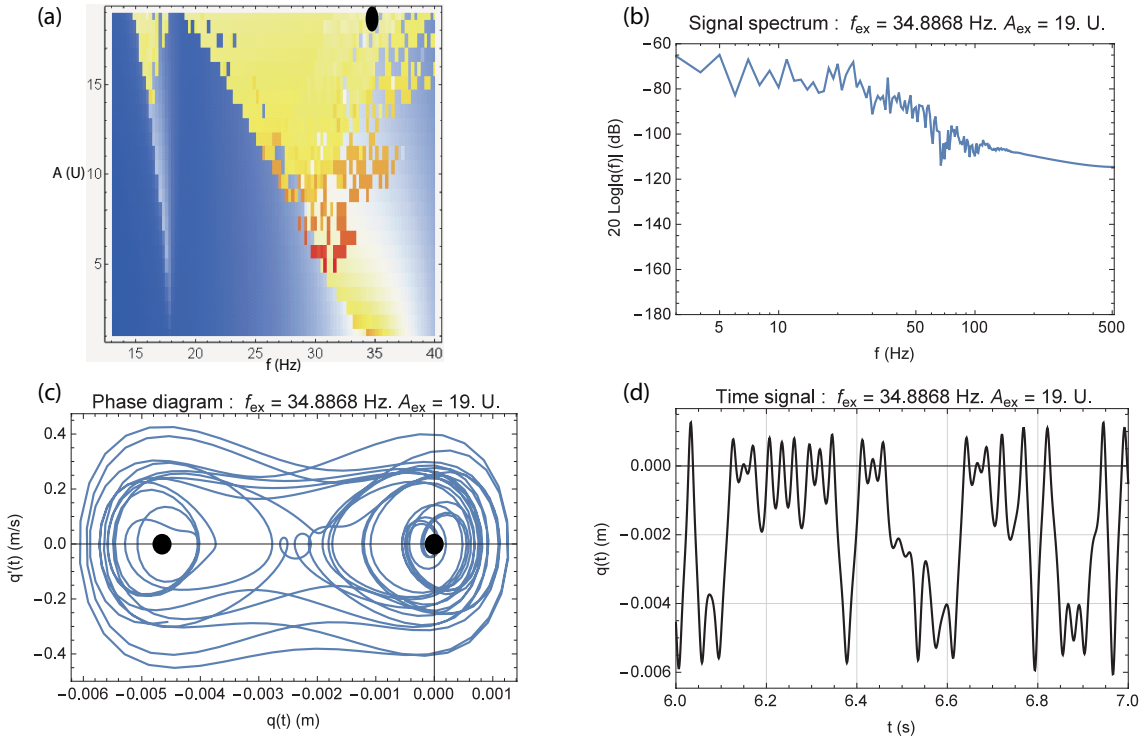

Figure 29: Computed BSA response. (a): density plot, the black oval represents the point of interest, (b): displacement spectrum, (c): phase plot, the black circles show the equilibrium points, (d): displacement time recording.